



Review

Metal-Polymer Nanoconjugates Application in Cancer Imaging and Therapy

André Q. Figueiredo¹, Carolina F. Rodrigues¹, Natanael Fernandes¹ , Duarte de Melo-Diogo¹,
Ilídio J. Correia^{1,*} and André F. Moreira^{1,2,*}

¹ CICS-UBI—Health Sciences Research Centre, Universidade da Beira Interior, Av. Infante D. Henrique, 6200-506 Covilhã, Portugal

² CPIRN-UDI/IPG—Centro de Potencial e Inovação em Recursos Naturais, Unidade de Investigação para o Desenvolvimento do Interior do Instituto Politécnico da Guarda, Avenida Dr. Francisco de Sá Carneiro, No. 50, 6300-559 Guarda, Portugal

* Correspondence: icorreia@ubi.pt (I.J.C.); afmoreira@fcsaude.ubi.pt (A.F.M.); Tel.: +351-275-329-002 (I.J.C.)

Abstract: Metallic-based nanoparticles present a unique set of physicochemical properties that support their application in different fields, such as electronics, medical diagnostics, and therapeutics. Particularly, in cancer therapy, the plasmonic resonance, magnetic behavior, X-ray attenuation, and radical oxygen species generation capacity displayed by metallic nanoparticles make them highly promising theragnostic solutions. Nevertheless, metallic-based nanoparticles are often associated with some toxicological issues, lack of colloidal stability, and establishment of off-target interactions. Therefore, researchers have been exploiting the combination of metallic nanoparticles with other materials, inorganic (e.g., silica) and/or organic (e.g., polymers). In terms of biological performance, metal-polymer conjugation can be advantageous for improving biocompatibility, colloidal stability, and tumor specificity. In this review, the application of metallic-polymer nanoconjugates/nanohybrids as a multifunctional all-in-one solution for cancer therapy will be summarized, focusing on the physicochemical properties that make metallic nanomaterials capable of acting as imaging and/or therapeutic agents. Then, an overview of the main advantages of metal-polymer conjugation as well as the most common structural arrangements will be provided. Moreover, the application of metallic-polymer nanoconjugates/nanohybrids made of gold, iron, copper, and other metals in cancer therapy will be discussed, in addition to an outlook of the current solution in clinical trials.

Keywords: metallic nanoparticles; metal-polymer nanoconjugates; cancer; photothermal effect



Citation: Figueiredo, A.Q.; Rodrigues, C.F.; Fernandes, N.; de Melo-Diogo, D.; Correia, I.J.; Moreira, A.F. Metal-Polymer Nanoconjugates Application in Cancer Imaging and Therapy. *Nanomaterials* **2022**, *12*, 3166. <https://doi.org/10.3390/nano12183166>

Academic Editor: Horacio Cabral

Received: 26 August 2022

Accepted: 9 September 2022

Published: 13 September 2022

Publisher's Note: MDPI stays neutral with regard to jurisdictional claims in published maps and institutional affiliations.



Copyright: © 2022 by the authors. Licensee MDPI, Basel, Switzerland. This article is an open access article distributed under the terms and conditions of the Creative Commons Attribution (CC BY) license (<https://creativecommons.org/licenses/by/4.0/>).

1. Introduction

The manipulation of matter at the nanoscale led to the development of various nanomaterials, based on polymers, lipids, ceramics, or metals, that exhibit exciting properties for improving the performance of electronics, medical diagnostics, and therapeutics [1,2]. Particularly, the application of nanoparticles for cancer therapy led to the development of new alternatives from therapeutics (i.e., drug delivery, photothermal and photodynamic effects) to diagnostic and imaging, leveraging the innate ability of these materials to accumulate in the tumor tissue [3–5].

In this field, the application of metallic-based nanomaterials (e.g., gold, iron, silver, and copper) has been capturing more attention in recent years due to their characteristic physical (e.g., magnetic behavior, plasmonic resonance, and imaging capacity) and chemical (e.g., radical oxygen species (ROS) generation, and catalytic activity enhancement) properties, which render them as platforms suitable for creating multifunctional cancer therapeutics [2,6–9]. Moreover, there are several methodologies described for the synthesis of metallic nanoparticles, such as physical or chemical vapor deposition, sol-gel methods, chemical reduction, hydrothermal methods, solvothermal method, laser ablation, and green synthesis processes, allowing the selection of the process most compatible with the available

laboratory/industrial conditions and desired physicochemical properties [10–13]. Additionally, metallic nanomaterials surface functionalization, a strategy often used to refine the therapeutics pharmacokinetics, can be performed by well-known and defined methodologies [14]. Thus, the metallic nanomaterials' theranostic potential provides an all-in-one solution for cancer diagnosis, therapy, and real-time monitoring, which ultimately can improve the therapeutic outcome of anticancer therapy [15,16]. This is the rationale behind various metallic-based nanomaterials under clinical trials, such as Aurolase[®], Nanotherm[®], and Magnablate[®].

Nevertheless, despite the wide number of publications showing the appealing features of metallic-based nanomaterials, their translation into the clinic is still very limited [17]. Such is widely associated with some toxicological issues, lack of colloidal stability, and the establishment of off-target interactions [18]. Additionally, when subjected to high-energy radiations, the metallic nanoparticles often undergo reshaping processes or are even degraded leading to the loss of their therapeutic potential [19]. Therefore, researchers have been exploring the combination of metallic nanoparticles with other materials, inorganic (e.g., silica) and/or organic (e.g., polymers). Particularly, the combination of the metallic nanoparticles' physicochemical properties with the superior biological performance of synthetic or natural polymers emerges as a valuable and straightforward approach to develop more effective anti-cancer therapeutics [16,20]. In this review, the application of metallic-polymer nanoconjugates/nanohybrids as a multifunctional all-in-one solution for cancer therapy will be summarized. Initially, the physicochemical properties rendering the metallic nanomaterials' potential to act as imaging and/or therapeutic agents will be summarized. Then, an overview of the main advantages of metal-polymer conjugation as well as the most common structural arrangements will be provided. Moreover, the application of metallic-polymer nanoconjugates/nanohybrids made of gold, iron, copper, and others in cancer therapy will be discussed, in addition to an outlook of the current solution in clinical trials.

2. Metallic Nanoparticles Applications and Therapies

Nanosized metals present optical and electrical properties that differentiate them from other nanomaterials, supporting their application in biomedicine, such as the development of biosensors (e.g., diagnosis of viruses using colloidal gold nanoparticles), bioimaging agents (e.g., iron oxide-based contrast agents), catalysts, mechanical reinforcement, and drug delivery system or other therapeutics. Moreover, these unique characteristics can be explored to create more effective antitumoral nanomedicines. The high density and X-ray attenuation capacity of metallic nanoparticles allow them the intrinsic capacity to be applied as contrast agents for bioimaging applications [21]. Up to now, several studies available in the literature have already shown that metallic nanoparticles provide a higher contrast enhancement in X-ray computed tomography (CT) imaging than the iodine-based contrast agents conventionally used in the clinic [22–26]. On the other hand, nanosized metals, such as gold, silver, and copper, show a pronounced plasmonic resonance phenomenon, i.e., the collective oscillation of the conduction band electrons in metal-based nanomaterials in response to the incident photons [27]. This interaction can lead to light absorption or scattering and is dependent on the size, morphology, distance, and dielectric constant of the metallic nanoparticles and surrounding medium [28–30]. In turn, the excited surface electrons can decay to the ground state via different processes (e.g., electron-to-photon, electron-to-electron, and electron-to-phonon energy conversion), the two most common events being the release of the absorbed energy in the form of light or heat [31]. The former is often explored to enhance the quantum efficiency and photostability of fluorophores, allowing the detection of lower quantities of biomarkers used in biosensing or bioimaging [32]. The latter is the foundation stone for the application of metallic nanoparticles in cancer hyperthermia/photothermal therapy [33]. However, it is essential to tailor the nanomaterials to interact specifically with near-infrared (NIR) radiation, a region of the spectra where the major biological components (e.g., collagen, hemoglobin,

and water) have the lowest or insignificant absorption [34]. This will reduce the off-target interactions and guarantee a site-specific activation of the metallic nanomaterials. Then, the heat generated by the light-nanoparticles interaction can mediate the destruction of the cancer cells [35,36]. The elevation of the tumor temperature to values superior to 45 °C provokes irreversible damage to cancer cells (e.g., DNA degradation, cell membrane disruption, protein denaturation), leading to cell death (i.e., tumor ablation). Otherwise, if mild temperature increases are achieved (i.e., between 40 and 45 °C), the cell damage is less pronounced and often reversed by the cell repair mechanisms [5,37,38]. Nevertheless, this creates a time window during which the cancer cells are more sensitive to the action of other therapeutic modalities such as chemotherapy [39]. Furthermore, metallic nanomaterials, such as those composed of iron, nickel, and cobalt, can also present magnetic properties, also allowing their application as contrast agents (magnetic resonance imaging (MRI)) and in tumor magnetic hyperthermia [40]. This capacity to be magnetically manipulated by external magnetic fields is also explored to guide these metallic nanomaterials in the human body and promote a tumor-specific accumulation [41,42]. At the tumor site, the utilization of alternating magnetic fields will promote the nanoparticles' vibration and consequently a localized temperature increase will be obtained [43].

Metallic nanomaterials have also shown the capacity to mediate the formation of ROS [18]. This oxidative stress can influence several cellular processes/structures, e.g., intracellular calcium concentrations, activate transcription factors, induce DNA damage, and lipid peroxidation (cell membrane disruption), and increased amounts of ROS are highly cytotoxic [18]. The mechanism of ROS generation by metallic nanomaterials is influenced by their physicochemical properties (e.g., size, chemical structure, surface area, and charge) [44]. Generally, metallic nanomaterials act as the reactant or catalyst for the reduction of molecular oxygen to water, which yields the production of ROS, such as superoxide radicals and hydroxyl radicals [45]. The ROS generation of metallic nanomaterials can be further boosted by light absorption [46]. During this process, the electrons transit to higher energy bands, facilitating the reaction with water or molecular oxygen and consequently the ROS generation, a process denominated by photodynamic effect [47,48].

Despite the imaging and therapeutic potential of metallic nanoparticles, the in vivo application and translation to the clinic are severely hindered by their low colloidal stability, high reactivity, the formation of the protein corona, and high cytotoxicity [49–51]. Therefore, to overcome these limitations, researchers have been combining the superior physicochemical features of metallic nanoparticles with the increased biological properties (e.g., biocompatibility, enhanced blood circulation time, targeting capacity) of synthetic and natural polymers, often referred to as metal-polymer nanocomplexes or nanohybrids.

3. Metal-Polymer Based Nanomaterials

The metal-polymer nanocomplexes or nanohybrids are a class of nanomaterials that aim to address the biological bottlenecks of the metallic nanoparticles' administration in humans. For that purpose, several strategies have been explored to create these new nanomaterials (Figure 1), namely the (i) surface coating of metallic cores (e.g., physical linkage and layer-by-layer), (ii) entrapment of metallic cores within polymeric matrices (e.g., nanoparticle in situ growth or post-synthesis entrapment), and (iii) the utilization of polymeric capsules [52–54]. One of the main rationales behind the introduction of polymers is to increase the colloidal stability of metallic nanoparticles and avoid protein adsorption during the nanoparticles' circulation in the blood [55,56].

Highly hydrophilic polymers are often associated with improvements in the nanoparticles' blood circulation time, namely by minimizing the nanoparticle-protein interaction, avoiding nanoparticles' aggregation as well as the size and charge changes, and reducing the recognition by the immune cells [57,58]. For this purpose, polymers, such as poly(ethylene glycol) (PEG), poly(oxazolines) (POX), and poly(zwitterion)s, have been excelling in enhancing the nanoparticles' blood circulation [59]. The PEG and POX anti-

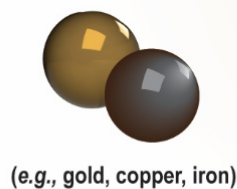
fouling properties, which are attributed to two main events, (i) the steric repulsion and (ii) the water barrier, impede the nanoparticles–proteins interaction, avoiding the formation of a protein corona that negatively impacts the nanomaterials' biological performance [60,61]. In turn, the zwitterionic polymers present overall electrostatic neutrality and high chain hydration that confer to them a stealthing capacity [62,63]. The higher blood circulation times associated with the utilization of these polymers will increase the nanomaterials' probability to accumulate and interact with the tumor cells, which can be essential for achieving superior antitumoral effects [64]. On the other hand, the natural and synthetic polymers can also imprint a stimuli-responsive (e.g., pH, temperature, and enzymatic) behaviour on the metallic-based nanomaterials, which can be particularly advantageous for controlling drug delivery [33,65–68]. In this regard, the heat generated by the nanomaterials (e.g., PTT and magnetic hyperthermia) can be also explored to induce phase changes in the polymers (e.g., Poly(N-isopropylacrylamide) (PNIPAM)) or increase their solubility, which will trigger the drug release [68,69]. Additionally, at the tumor site, the metal-polymer nanocomplexes/nanohybrids will also have an impact on the physiological conditions that can be explored to trigger the drug release, such as an acidic pH, overexpression of certain enzymes (e.g., matrix metalloproteinases), and an increased RedOx environment [65,67,70]. Apart from the passive accumulation of the nanomaterials at the tumor site, usually dependent on the enhanced permeability and retention (EPR) effect, the polymers or other targeting moieties can confer a specific recognition of molecules overexpressed in the tumor tissue [5,71]. This higher specificity towards cancer cells will favor the accumulation of nanomaterials in these areas as well as the nanomaterials–cancer cell interaction [72]. Therefore, the metal–polymer nanocomplexes or nanohybrids show the potential to create novel and more effective anticancer therapeutics. In the following section, the application of metallic–polymer nanoconjugates/nanohybrids made of gold, iron, copper, and others in cancer therapy will be overviewed, showing the therapeutic modalities that each metal nanoparticle allows to explore.

3.1. Gold-Polymer Conjugates

Gold nanoparticles are one of the most explored metallic nanomaterials for biomedical applications, from bioimaging to drug delivery [73–75]. The applicability of gold nanomaterials in bioimaging is demonstrated in different works in the literature, principally as a contrast agent for CT imaging [76]. For example, Xi and co-workers observed that, when an X-ray beam of 100 KeV is used, gold nanoparticles present an absorption coefficient two-times superior to that obtained with iodine (a conventional contrast agent used in the clinic) [77]. In turn, the pronounced surface plasmon resonance of gold nanoparticles has been supporting the development of novel photothermal therapies for cancer therapy (Table 1). This phenomenon can be fine-tuned to enhance the gold nanoparticles' absorption in the NIR region (700–1100 nm) by optimizing the nanoparticles' size and/or shape (e.g., spheres, cages, stars, and rods) [37,78]. Per se, the application of gold nanospheres in cancer photothermal therapy (PTT) is limited since its absorption peak is in the 500–550 nm region [79]. However, the organization of gold nanospheres in nanoclusters or shells renders a shift in the absorption spectra to the NIR region [2,5]. This change in the gold nanoparticles' optical properties is attributed to the coupling of the plasmon resonance of adjacent gold nanospheres [80]. Therefore, the fine-tuning of the gold nanoclusters or shells' absorption spectra can be achieved by optimizing the nanospheres' size and interparticle distance [2]. In turn, the surface plasmon resonance in non-spherical gold nanoparticles varies with the nanoparticle surface [81,82]. For example, the two different surfaces in gold nanorods, longitudinal and transversal surfaces, originate two absorption bands. The transversal surface leads to an absorption band in the 500–550 nm region of the spectra, whereas the longitudinal surface originates an absorption peak that can be fine-tuned from the visible to the NIR region of the spectra [83,84]. This peak generated by the longitudinal surface resonance is determined by the aspect ratio of gold nanorods (i.e., quotient between length and width) [85]. Otherwise, the surface plasmon resonance of gold nanostars

is defined by the particle's core size, the number of tips, as well as the tips' length and width [2]. Therefore, the gold nanoparticles' plasticity and fine-tuning ability to present a high absorption efficiency in the NIR region of the spectra propelled their application in the cancer PTT. Nevertheless, despite the theragnostic potential of gold nanoparticles, their direct application in the human body is hindered by their high affinity to establish interactions with thiol groups, which favors the interaction with different biomolecules and lead to the nanoparticles' aggregation [80]. Moreover, the gold nanoparticles can also be degraded when exposed to high-energy radiations, such as those used in CT imaging and PTT, causing the loss of their bioactivity [86]. Furthermore, several reports in the literature also describe that gold nanoparticles are strongly accumulated in the kidneys, causing nephrotoxicity, and may also trigger the lysis of red blood cells [78]. To address these issues, researchers have been exploring the development of gold-polymer nanocomplexes or nanohybrids to increase colloidal stability, biocompatibility, and even tumor specificity.

Metallic-based Nanomaterials



(e.g., gold, copper, iron)

Advantages:

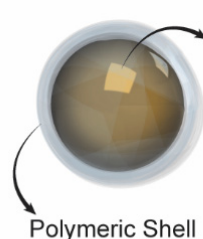
- Imaging capacity;
- Plasmonic resonance;
- Magnetic behavior;
- Photothermal capacity;
- Radical oxygen species generation;
- Catalytic activity enhancement;

Problems:

- Toxicological issues;
- Off-target interactions (e.g., blood proteins);
- Lack colloidal stability;
- Reshaping and degradation processes under high-energy radiations;

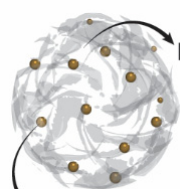
Loss of the therapeutic potential

Metal-Polymer based Nanomaterials



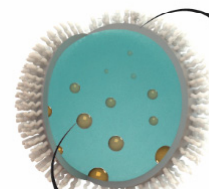
Polymeric Shell

Metal core



Entrapped metallic cores

Polymeric matrix



Entrapped metallic cores

Polymeric capsule

Polymers (e.g., natural polymers, PEG, Polyoxazolines) incorporation:

- Targeting capacity;
- Increase biocompatibility;
- Increase the colloidal stability;
- Protection from degradation and reshaping;
- Reduce the interaction with proteins and immune system;

Enhanced

*Blood Circulation Time
Tumor Accumulation
Therapeutic Effect*

Figure 1. Overview of the properties of metallic nanoparticles, advantages of the polymers' inclusion, and representation of the most common structural organizations of the metal-polymer nanohybrids/complexes.

Table 1. Gold-based metallic-polymer nanoconjugates/nanohybrids, their physicochemical properties, and therapeutic applications (N.D.—non disclosed, N.A.—not applicable).

Metal	Morphology	Modification	Size (nm)	Surface Charge (mV)	Loading	In Vitro	In Vivo	Application	Ref.
Gold	Rods	UCST polymer (P(AAm-co-AN)-DDAT), metalloproteinase 2 (MMP-2)-sensitive peptides	Length \approx 48.04; Width \approx 12.08	N.D.	Doxorubicin (DOX)	HepG2 cells	HepG2 tumor-bearing mice	PTT (λ_{ex} = 808 nm) and chemotherapy	[33]
		Mesoporous silica; D- α -Tocopherol polyethylene glycol 1000 succinate (TPGS), and Hyaluronic acid (HA)	Length \approx 85; Width \approx 64	-3 ± 5 and -10 ± 4 for TPGS/HA ratios of 1:1 and 4:1, respectively	N.A.	HeLa cells	N.A.	PTT (λ_{ex} = 780 nm)	[86]
		Mesoporous silica, HA, and polyethyleneimine (PEI)	Length: 88 ± 5 ; Width: 63 ± 5 ;	-10 ± 2	Acridine Orange (AO)	HeLa cells	N.A.	PTT (λ_{ex} = 750 nm) and chemotherapy	[87]
	Spheres	Poly(ethylene glycol) (PEG) and Lactoferrin (LF)	5	N.D.	N.A.	Caco-2, U87MG cells	GBM tumor-bearing mice	PTT (λ_{ex} = 532 nm)	[54]
	Stars	Polydopamine (PDA) and Folic acid (FA)	149 ± 3	-19 ± 2.7	DOX	MCF-7, MCF-7/ADR, NIH/3T3, and HaCaT cells	MCF-7/ADR bearing mice	PTT (λ_{ex} \approx 800 nm) and chemotherapy	[56]
		Dendritic polyglycerol (dPG) and HA	68.1	13.9	Retinoic acid (RA)	MDA-MB-231 cells	4T1 tumor-bearing mice	PTT (λ_{ex} \approx 800 nm) and chemotherapy	[88]
PEG and CD133 antibody		\approx 120	-22.47	IR780/DTX	PC3 cells	PC3 tumor-bearing mice	PTT (λ_{ex} = 810 nm), PDT, and chemotherapy	[89]	
Cages	Poly (acrylic acid) (p _A) or Poly(NIPAM-co-AM) (p _N)	for p _A (Au) \approx 130; N.D. for p _N (Au)	\approx -4 for p _A (Au) formulation at pH 7.4; N.D. for p _N (Au) formulation	p _A (Au)-loaded with Erl and p _N (Au) loaded with DOX	A431 or MCF-7 cells	A431 or MCF-7 tumor-bearing mice	PTT (λ_{ex} \approx 800 nm for both formulations) and chemotherapy	[68]	
	PVP, PEG, and anti-heat shock protein (HSP) monoclonal antibody	61.2 ± 4.85	-8.2 ± 1.25	N.A.	4T1	4T1 tumor-bearing mice	PTT (λ_{ex} \approx 808 nm)	[90]	

Abbreviations—PDT: Photodynamic Therapy; PTT: Photothermal Therapy.

Peng and colleagues demonstrated the applicability of gold-based nanomaterials in bioimaging by following the biodistribution and tumor accumulation of PEGylated dendrimer-entrapped gold nanospheres [91]. In fact, the authors reported that these nanomaterials have an attenuation intensity higher than Omnipaque (an iodine-based contrast agent), which allowed them to follow the PEGylated dendrimer-entrapped gold nanoparticles in the blood circulation, after intravenous injection, as well as to perform the CT imaging of SPC-A1 xenograft tumors. Moreover, the authors reported that the PEGylated dendrimer-entrapped gold nanoparticles had a half-decay time in the blood circulation of 31.76 h, which was 2.5 times higher than that of bare gold nanorods previously reported. Furthermore, Gu et al. produced RGD-modified mPEG-PLGA nanocapsules containing gold nanoclusters and indocyanine green for the imaging and PTT of breast cancer [92]. The loaded mPEG-PLGA nanocapsules were formed via a water-in-oil-in-water emulsion using sonication, where (i) the first emulsion consisted of the water phase with gold nanoclusters and the oil phase with indocyanine green and the mPEG-PLGA. In the second emulsion, the mPEG-PLGA nanocapsules were further modified with poly(vinyl alcohol) and poly(acrylic acid), allowing the subsequent functionalization with RGD peptide via carbodiimide chemistry. The authors demonstrated that both one-photon and two-photon imaging techniques could be used to follow the nanocapsules in 4T1 tumor-bearing BALB/c mice. Moreover, the RGD-modified nanocapsules showed a preferential accumulation in

U87-MG cancer cells (overexpressing $\alpha v \beta_3$ integrins), when compared to MCF-7 cancer cells (low expression of $\alpha v \beta_3$ integrins), leading to the almost complete ablation of the cancer cells after irradiation with a NIR laser (808 nm, 2 W cm^{-2} , for 5 min). Feng and co-workers developed two different tumor-targeted gold nanocages for the combinatorial chemo-PTT of breast cancer [68]. For that purpose, pH-responsive gold nanocages were formulated via electrostatic interaction between the poly(acrylic acid) and the surface of the particles, entrapping the gold particles in the polymeric chains ($p_A\text{Au}$ nanoparticles) and loaded with Erlotinib (Erl), an epidermal growth factor receptor (EGFR) inhibitor. In turn, temperature-responsive gold nanocages were produced by reacting them with the thiol-terminated N-isopropylacrylamide (NIPAM) and acrylamide (AM) ($p(\text{NIPAM-co-AM})$ co-polymer ($p_N\text{Au}$ nanoparticles) and subsequently loaded with doxorubicin (Dox). The $p_A\text{Au}$ nanoparticles showed a pH-triggered Erl release due to the protonation of poly(acrylic acid) in acidic pH (i.e., loosening of the polymeric barrier), 4.5%, 24.8%, 44.1%, or 66.3% Erl released after 6 h at pH 7.4, 6.5, 6, or 5. Otherwise, the Dox-loaded $p_N\text{Au}$ nanoparticles were responsive to the irradiation with a NIR laser (808 nm, 0.5 W cm^{-2} , for 10 min) and consequent increase in temperature (i.e., superior to 45°C , a value higher than the lower critical solution temperature). The authors reported 46.2% of Dox released in 10 h, after a 10 min NIR laser irradiation, contrasting with the 5% detected in the absence of NIR irradiation. The in vivo studies performed in MCF-7 and A431 tumor-bearing mice demonstrated a passive and preferential accumulation in the tumor tissue (Figure 2). Moreover, the combinatorial therapy led to the reduction of A431 tumors' size by 98%, after 14 days, whereas in MCF-7 tumors (low expression of EGFR), these nanomaterials only slowed the tumor growth.

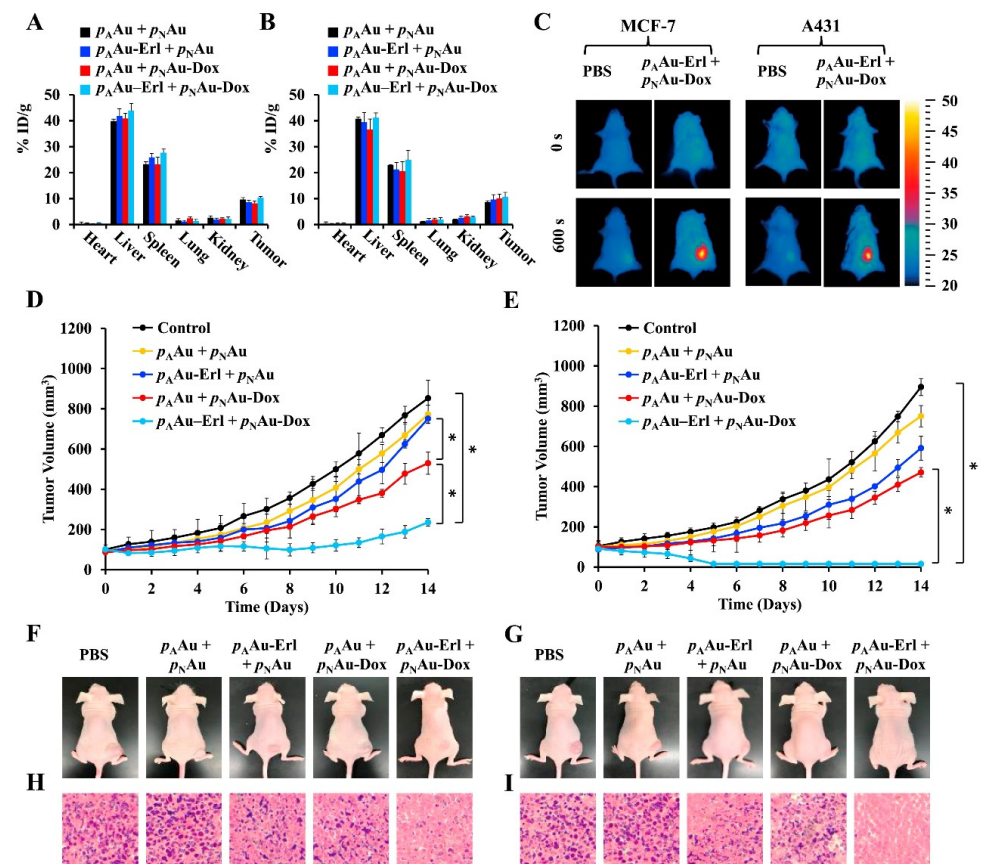


Figure 2. In vivo evaluation of the $p_A\text{Au-Erl}$ plus $p_N\text{Au-Dox}$ antitumoral efficacy. Biodistribution analysis of $p_A\text{Au} + p_N\text{Au}$, $p_A\text{Au-Erl} + p_N\text{Au}$, $p_A\text{Au} + p_N\text{Au-Dox}$, and $p_A\text{Au-Erl} + p_N\text{Au-Dox}$ ($12.4 \text{ Au mg kg}^{-1}$ of mouse, Erl:Dox = 1:1) in MCF-7 (A) and A431 (B) tumor-bearing mice. Infrared thermal images of MCF-7 and A431 tumor-bearing mice before and after NIR laser irradiation

(808 nm, 0.5 W cm^{-2} , for 10 min) (C). Analysis of the tumor growth curve in MCF-7 (D) and A431 (E) tumor-bearing mice. * $p < 0.05$ analysed by ANOVA. Photos and histological analysis of MCF-7 (F,H) and A431 (G,I) tumor-bearing mice. Reprinted with permission from [68]. Copyright (2019) Elsevier.

3.2. Iron-Polymer Conjugates

The utilization of iron oxide nanoparticles can be explored in different biomedical applications, such as drug delivery, hyperthermia, and magnetic resonance imaging. Similar to gold nanoparticles, iron oxide can be produced in different shapes, such as spherical, rod-like, and cubical [93,94]. These nanoparticles (Fe_2O_3 and Fe_3O_4), when their size is inferior to 20 nm, present a superparamagnetic behavior at room temperature, i.e., the magnetization of the nanoparticles is close to 0 in the absence of an external magnetic field [95,96]. The iron oxide nanoparticles magnetism allows for widespread application in cancer therapy (Table 2), namely as contrast agents for magnetic resonance imaging: Feridex[®], Resovist[®], and Endorem[®]. The data available in the literature indicate that iron oxide nanoparticles are less toxic than the conventionally used gadolinium-based contrast agents, without presenting significant losses in imaging capacity [95]. Moreover, the magnetic properties of iron oxide nanoparticles have also been explored to direct the accumulation of the nanoparticles, specifically towards the tumor tissue, and in certain cases mediate a hyperthermic effect [97,98]. The former explores the application of an external magnetic field to guide the nanoparticles and promote their accumulation in the target tissue [99]. The latter employs an alternating magnetic field to induce the oscillation of iron oxide nanoparticles, which in turn generate heat [97]. This hyperthermic effect is dependent on the magnetic properties of the nanoparticles as well as on the frequency and intensity of the alternating magnetic field [100,101]. However, the biological application of iron oxide nanoparticles is hindered by their limited colloidal stability, tending to agglomerate when in contact with biological fluids [102]. With this in mind, Xu et al. prepared GSH-responsive hyaluronic acid-coated small iron oxide nanoparticles (HIONPs) for the diagnosis of liver metastases [103]. The nanoparticles were formed via a one-pot method, promoting the oxidation of ferrous ions to create iron oxide nanoparticles that were coated with hyaluronic acid modified with dopamine through the establishment phenol–metal coordination interactions. The in vitro measurements in a 0.52 T NMR instrument showed that the HIONPs have a longitudinal proton relaxivity (r_1) of $41.3 \text{ Fe mM}^{-1} \text{ s}^{-1}$, indicating the applicability of HIONPs as T_1 MRI contrast agents. This was confirmed using a 3 T MR scanner where the HIONPs led to higher T_1 -weighted magnetic resonance signals and lower T_2 -weighted magnetic resonance signals when the Fe concentration increased from 0 to 0.2 mM. Moreover, the application of HIONPs ($\text{Fe} = 0.03 \text{ mmol kg}^{-1}$) in mice with B16F10, 4T1, and CT26 liver metastases allowed the metastases detection via MRI, showing the highest contrast-to-noise ratio 1 h after injection. This capacity is attributed to the higher GSH concentration in the mice liver tissue (i.e., 11 to 76-times higher) when compared to the tumor/metastases. The higher GSH concentration promotes the removal of the hyaluronic acid coating and consequent nanoparticle aggregation, which led to a significant decrease in the r_1 value. In this way, the hepatic tissues became dark whereas the tumor/metastases are bright in the MRI. Moreover, the authors also described that the HIONPs presented a higher imaging capacity than Primovist[®] (Gd-based imaging agent), where the metastases and surrounding liver tissue presented a similar contrast-to-noise ratio. In another work, Xiao and co-workers developed ultrathin vesicles with multimodal imaging capacity for the combinatorial chemo-PTT of cancer [104]. For that purpose, ultrasmall superparamagnetic iron oxide nanoparticles, cisplatin, and liquid perfluorohexane were encapsulated in PLGA nanovesicles, followed by the formation of an ultrathin silica layer to prevent leakage. Then, the surface of the particles was modified with polyaniline (a photothermal agent) and functionalized with R8-RGD. In these nanoparticles, the iron oxide acted as a

T_2 -weighted magnetic resonance contrast agent, with a transverse relaxivity (r_2) value of $258.5 \text{ Fe mM}^{-1} \text{ s}^{-1}$, three times superior to the iron oxide nanoparticles alone. Moreover, the in vivo studies in A549 tumor-bearing mice showed that the administration of the PLGA vesicles containing the iron oxide nanoparticles allows the monitoring of the changes in the tumor cellularity via MRI. Additionally, the chemo-photothermal combinatorial treatment led to a significant regression, close to 97%, of the tumor volume in 21 days. Chen and colleagues produced a dual-targeted magnetic iron oxide nanoparticle for the imaging and hyperthermia of breast tumors (Figure 3) [105]. The iron oxide nanoparticles were coated with a DSPE-PEG2000 shell and then modified with RGDyK (neovascular endothelium targeting) and D-glucosamine (glucose transporter affinity) via carbodiimide chemistry. The authors observed that the combination of magnetic and active targeting approaches resulted in the best contrast effect on T_2 -weighted MRI from 3 to 48 h, showing the tumor region completely dark due to the accumulation of the nanoparticles. The tumor/normal tissue signal ratio at 48 h for active targeting strategies was 0.6 whereas for the magnetic plus active targeting combination this value was inferior to 0.3, showing a higher difference in the signal obtained in the tumor and normal tissues. Moreover, the utilization of alternating current magnetic fields ($1.485 \times 10^9 \text{ Am}^{-1} \text{ s}^{-1}$), focused on the tumor region, induced a temperature increase to $44 \text{ }^\circ\text{C}$, which successfully slowed the growth of 4T1 tumors when compared to the control group (i.e., the relative tumor volume of 500% and 200% for control and iron oxide groups, respectively).

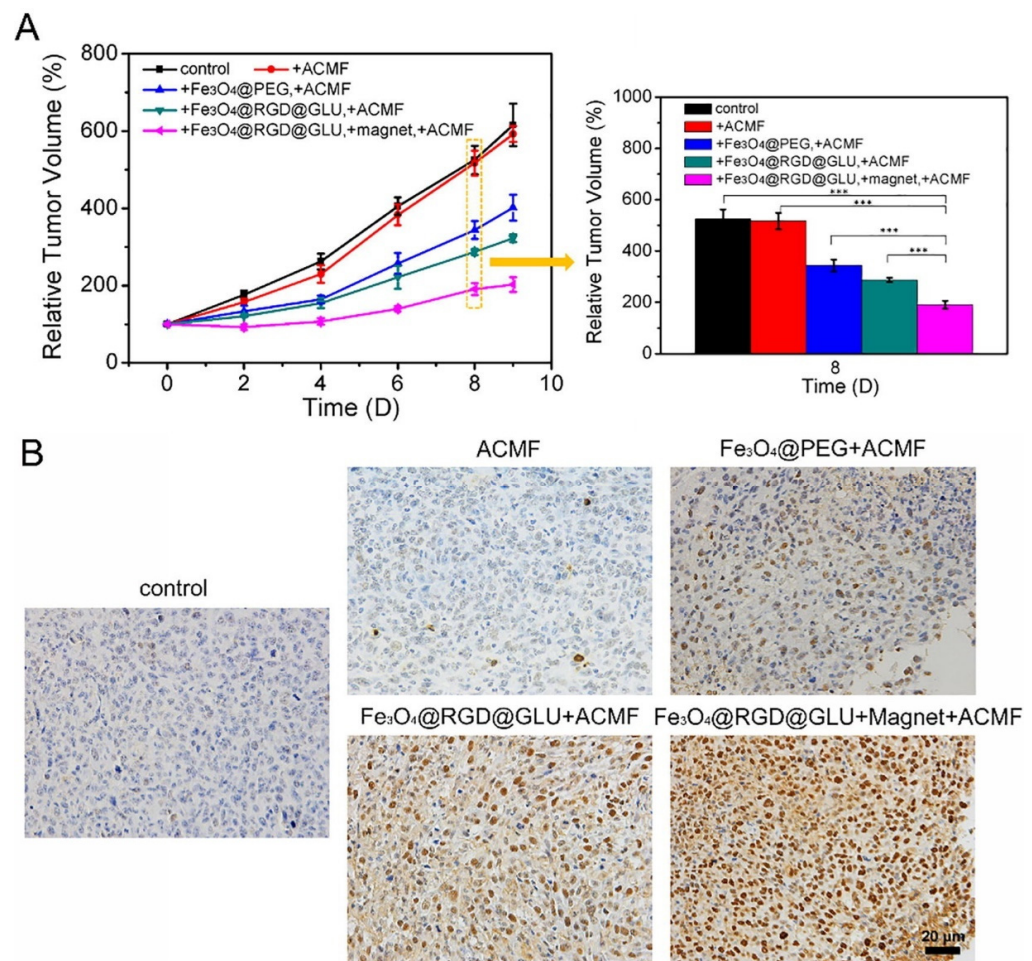


Figure 3. Analysis of the tumor growth curves for 10 days after treatment with iron oxide nanomaterials, mean \pm SE and $n = 5$ (A). TUNEL histological analysis of mice tumors at day 9. Statistical significance is represented by the asterisk (***) $p < 0.001$. TUNEL assay for mice tumors on day 9 following various treatments (B). Reprinted with permission from [105]. Copyright (2019) Elsevier.

Table 2. Iron-based metallic-polymer nanoconjugates/nanohybrids, their physicochemical properties, and therapeutic applications (N.D.—non disclosed, N.A.—not applicable).

Metal	Morphology	Modification	Size (nm)	Surface Charge (mV)	Loading	Longitudinal/Transverse Proton Relaxivity	In Vitro	In Vivo	Applications	Ref.
Iron	Ring	GO (graphene oxide) and CREKA (Cys-Arg-Glu-Lys-Ala)	223.3	22 ± 0.4	N.A.	N.D.	4T1 cells	4T1 tumor-bearing mice	MTD and MTT	[6]
	Spheres	HA conjugated with dopamine (HA-DA)	60.7	−16	N.A.	r_1 : 41.3 mM ^{−1}	A549, HepG2, CT26, B16F10, and 4T1 cells	4T1, B16F10, and CT26 tumor-bearing mice	MRI	[103]
		PLGA, silica, Polyaniline (PANI), and R8-RGD	206	22.8	Cisplatin	r_2 : 258.5 mM ^{−1} s ^{−1}	A549 cells	A549 tumor-bearing mice	PTT (Strong Absorption in NIR region), MRI, and chemotherapy	[104]
		PEG, RGD, D-Glucosamine	32.31 ± 0.71	−30.2 ± 0.76	N.A.	r_2 : 554 mM ^{−1} s ^{−1}	4T1 cells	4T1 tumor-bearing mice	MRI and hyperthermia	[105]
		PEI, PLGA, and HA	159.5 ± 2.3	−9.1	Olaparib (Olb)	Saturation magnetizations: 21.08 emu/g	MDA-MB-231 cells	MDA-MB-231 tumor-bearing mice	RMF and chemotherapy	[106]
		PLGA, gold shell, and Herceptin	285.7 ± 81.4	N.D.	DOX	r_2 : 345.31 ± 23.06 mM ^{−1} s ^{−1}	BT474, MCF, and BT474/Adr cells	BT474 tumor-bearing mice	MRI, PTT ($\lambda_{ex} \approx 750\text{--}800$ nm), and chemotherapy	[107]
		AS1411 and PLGA	201.87 ± 1.60	−10.67 ± 0.25	N.A.	N.D.	MCF-7 cells	MCF-7 tumor-bearing mice	PA/US imaging and PTT ($\lambda_{ex} = 635$ nm),	[108]
		HA-SS-PLA	≈11	N.D.	PTX	N.D.	HeLa cells	HeLa tumor-bearing mice	Chemotherapy	[109]
	Sheets	PDA (polydopamine), and rGO (reduced graphene oxide)	251	−27.5	N.A.	N.D.	MCF-7 cells	N.A.	MRI, PTT (Strong Absorption in NIR region), and PDT	[110]

Abbreviations—MRI: Magnetic Resonance Imaging; MTD: Magnetothermodynamic therapy; MTT: Magnetothermal Therapy; PA: Photoacoustic Imaging; PDT: Photodynamic Therapy; PTT: Photothermal Therapy; RMF: Rotating Magnetic Field Therapy; US: Ultrasound Imaging.

3.3. Copper-Polymer Conjugates

Copper nanomaterials have emerged in recent years as promising inorganic nanoparticles for biomedical applications (Table 3). Copper is a transition metal and can be engineered to form various nanomaterials, such as copper oxides, copper selenides, and copper sulfides [111–113]. Among them, copper sulfides have been the most explored due to the simple synthesis process and high NIR absorbing capacity, allowing their application in cancer PTT [37]. On the other hand, the copper nanomaterials can also be used as Fenton-like reagents mediating the formation of ROS (chemodynamic therapy) [114]. Moreover, the generation of ROS can also be stimulated under light irradiation (photodynamic therapy (PDT)) [115]. However, copper is often defined as more toxic than iron and gold, which makes the release of copper ions in the human body undesirable [116,117]. With that in mind, Li et al. showed that the surface functionalization with an amphiphilic polymer, poly(isobutylene-alt-maleic anhydride) (PMA), enhances the colloidal stability of copper telluride nanoparticles without visible agglomeration for periods longer than one month [118]. Furthermore, *in vitro* studies performed in 3T3 fibroblasts showed significant cytotoxicity after irradiation with a NIR laser (830 nm, 0.5 mW cm⁻², for 2 s). In another work, Li and colleagues developed a PEGylated copper sulfide nanoparticle for the simultaneous PDT and PTT of lung cancer (Figure 4) [119]. For that purpose, thiolated-PEG was reacted with the copper sulfide nanoparticles rendering the PEGylated nanoparticles. The authors observed that the nanoparticles' irradiation (30 µg mL⁻¹) with a NIR laser (808 nm, 1 W cm⁻², for 10 min) reaches temperatures superior to 42 °C. Moreover, the authors also observed the continuous quenching of the p-nitrosodimethylaniline (RNO) absorption under NIR irradiation, indicating the generation of ROS during this period. Moreover, the *in vivo* studies in SPC-A-1 tumor-bearing mice showed that the combination of PDT and PTT decreases tumor growth, observing a 5% increase in the tumor volume at day 14 after administering PEGylated copper sulfide nanoparticles (30 µg mL⁻¹) plus NIR. Similarly, Shi et al. produced a PEGylated copper sulfide nanoparticle modified with RGD to target metastatic gastric cancer [120]. The nanoparticles were formed by the reaction of thiolated-PEG-COOH and copper sulfide, followed by the RGD modification using carbodiimide chemistry. The obtained nanoparticles showed computed-tomography contrast capacity similar to the Iodixanol (a clinically used contrast agent). Furthermore, the irradiation of the nanoparticles (60 µg mL⁻¹) with a NIR laser (808 nm, 1 W cm⁻², for 5 min) led to a temperature increase to 60 °C. In the *in vivo* studies, the authors observed that the RGD-modified PEGylated copper sulfide nanoparticles allowed the identification of MKN45 tumors and metastasis in sentinel lymph nodes through T₂-weighted magnetic resonance images. Moreover, the NIR laser irradiation (808 nm, 1 W cm⁻², for 10 min) promoted the increase in tumor/metastases temperature to 57 °C, leading to the complete ablation of the metastatic MKN45 tumors (sentinel lymph nodes weight similar to the healthy ones, 2.5 mg).

Table 3. Copper-based metallic-polymer nanoconjugates/nanohybrids, their physicochemical properties, and therapeutic applications (N.D.—non disclosed, N.A.—not applicable).

Metal	Morphology	Modification	Size (nm)	Surface Charge (mV)	Loading	In Vitro	In Vivo	Applications	Ref.
Copper	Spheres	Lanthanide-doped nanoparticles and PEG	45	N.D.	N.A.	HeLa cells	Cervical cancer tumor xenograft	NIR-II luminescence imaging/CT/MRI, CDT, and PDT	[121]
		P-(OEOMA-co-MEMA)	285	-17.2	TAPP	CT26 cells	CT26 tumor-bearing mice	PA/PI, PTT (Band from visible to NIR), PDT, and SDT	[122]
		DSPE-PEG modified with Lanreotide	186.1 ± 5.2	-16.4 ± 0.1	Docetaxel	PC-3 cells	PC-3 tumor-bearing mice	PA, PI, PTT (Band between 700 and 1000 nm), PDT, and chemotherapy	[123]

Table 3. Cont.

Metal	Morphology	Modification	Size (nm)	Surface Charge (mV)	Loading	In Vitro	In Vivo	Applications	Ref.
		PLGA, PDA, and PEG	288 (Higher MW-PLGA); 257 (Lower MW-PLGA)	−18.7 (Higher MW-PLGA); −22.2 (Lower MW-PLGA)	N.A.	Cal-33 cells	N.A.	MRI, PTT (N.D.), and chemotherapy	[124]
		HA/PEI	330.7	16.9	Disulfiram	Eca109	Eca109 tumor-bearing mice	Chemotherapy and FL	[125]
		PEG-NH ₂ and PCL-SS-P(DPA/GMA/MP)	151.5 ± 2.2	−17.1 ± 1.7	Dox	L929 and 4T1	4T1 tumor-bearing mice	PTT (Strong absorption in the NIR region), and chemotherapy	[126]
		HA and PDA	106	−19.43	Dox	HeLa and 4T1	4T1 tumor-bearing mice	PA, PTT (N.D), CDT, and chemotherapy	[127]
Framework		Pluronic F127	186.4 ± 16.7	−1.2 ± 0.1	O ₂	4T1 and HeLa cells	4T1 tumor-bearing mice	PDT (Band from visible to NIR)	[128]
	Cubes	BSA and PEG-FA	60	N.A.	N.A.	HepG2 cells	N.A.	PTT (Band from visible to NIR) and chemotherapy	[129]

Abbreviations—CT: Computed Tomography; PA: Photoacoustic Imaging; PDT: Photodynamic Therapy; PTT: Photothermal Therapy; SDT: Sonodynamic Therapy.

3.4. Other Metal-Polymer Nanoconjugates

Apart from the previously presented gold-, iron-, and copper-based nanomaterials, other metals have also been explored to create novel and more effective anticancer therapeutics (Table 4). Zinc-based nanoparticles, particularly zinc oxide (ZnO), are considered relatively biocompatible and generally regarded as safe. These nanoparticles present photoluminescence properties and a band gap that facilitates the interaction with oxygen and hydroxyl ions prompting the generation of superoxide and hydroxyl radicals (Table 4) [130,131]. Moreover, this ROS generation shows a certain selectivity towards cancer cells, decreasing the potential for inducing side effects [132]. Song and co-workers functionalized ZnO nanoparticles with polyvinylpyrrolidone for application in the imaging and therapy of colon cancer [133]. These authors reported that the surface functionalization maintained the stability of nanoparticles for 14 days, whereas non-coated ZnO nanoparticles aggregated after three days, without impacting the ROS generation capacity. Moreover, the authors also observed that the administration of the polyvinylpyrrolidone coated ZnO nanoparticles, at a concentration of 50 µg mL^{−1}, reduced the viability of SW480 cancer cells to 54% due to ROS generation. In turn, the ROS generation was boosted by the irradiation with UV light, with cell viability of 15% at a concentration of 50 µg mL^{−1} (IC₅₀ of 21.688 µg mL^{−1}). This PDT capacity was also observed in the SW480 tumor-bearing mice, where the nanoparticles plus light treatment slowed the tumor growth for 28 days, a tumor inhibition rate of 61.1%.

Platinum (Pt) is a catalytic noble metal that has been explored in cancer therapy, namely in the form of chemotherapeutic drugs containing platinum atoms, such as cisplatin and derivatives [134]. The utilization of platinum nanoparticles is focused on the release of platinum ions that will induce DNA damage and provoke cell death [135]. Additionally, the platinum nanoparticles can also mediate the generation of ROS or act as photothermal agents [136,137]. Chen and colleagues developed PEGylated porous platinum nanoparticles loaded with Dox for application in breast cancer therapy [138]. In the synthesis process, Pluronic F127 was used as a surfactant for the platinum nanoparticles and then reacted with thiolated-mPEG. This surface modification enhanced the solubility and stability of the platinum nanoparticles. Moreover, the authors also reported that the presence of a 10 mHz square wave AC field (10 mA) further enhanced the ROS generation capacity. In turn, the combination of Dox delivery and ROS generation induced the regression of 4T1 tumors, showing a tumor growth inhibition of 95.5% after 14 days. Zhu and co-

workers prepared sodium hyaluronate stabilized platinum nanoparticles (HA/Pt) for mediating a photothermal effect [139]. Apart from the nanoparticle stabilization, the HA functionalization increased the nanoparticles' specificity towards the MDA-MB231 cancer cells (overexpression of CD44), when compared to the uptake by NIH3T3 cells (low expression of CD44). Furthermore, the *in vivo* studies in MDA-MB231 tumor-bearing mice revealed that upon irradiation with a NIR laser (808 nm, 1 W cm⁻¹, for 10 min), the HA/Pt nanoparticles induced an increase in the temperature of the tumor to 44 °C, which translated to a reduction in the tumor growth for 14 days.

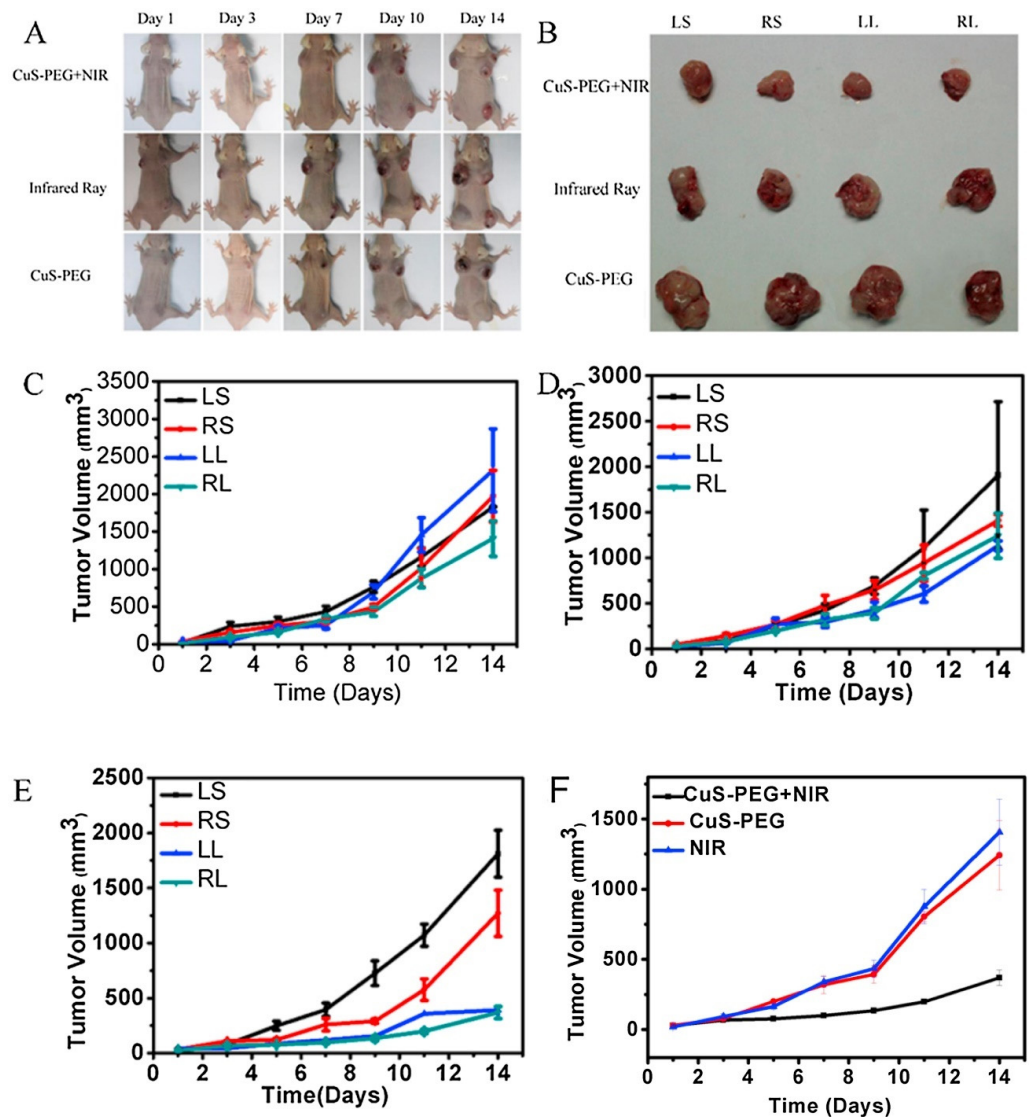


Figure 4. Photos of the tumor-bearing mice at 1, 3, 7, 10 and 14 days (A) and SPC-A-1 tumors at day 14 (B) after the treatment of the nanomaterials. Tumor growth curves in the control group; 0 μL CuS-PEG in LS, 30 μL CuS-PEG in the RS, 50 μL of CuS-PEG in the LL, and 100 μL CuS-PEG in the RL (C). Tumor growth curves in the NIR—irradiated group; 0 μL NS in the LS, 30 μL NS in the RS, 50 μL NS in the LL, and 100 μL NS CuS-PEG in the RL (D). Tumor growth curves in the CuS-PEG + NIR group, 100 μL NS in the LS, 30 μL CuS-PEG in the RS, 50 μL CuS-PEG in the LL, and 100 μL CuS-PEG in the RL (E). Tumor growth volume curve comparison for 100 μL (30 μg/mL) CuS-PEG +NIR in the RL; 100 μL (30 μg/mL) CuS-PEG in the RL, and 100 μL NS in the RL (F). LS—left shoulder administration; RS—right shoulder administration; LL—left leg administration; RL—right leg administration; NS—normal saline solution. Reprinted with permission from [111]. Copyright (2017) Elsevier.

Silver (Ag) is a noble metal with vast applications, being widely applied in the biomedical field as an antimicrobial agent [140]. The silver nanoparticles can mediate ROS formation and consequently induce lipid peroxidation, protein oxidation, and DNA damage [141,142]. Park and co-workers developed indocyanine green-loaded silver nanoparticles functionalized with PEG and BSA for application in cancer PTT [143]. The BSA was used to stabilize the produced silver nanoparticles, followed by the reaction with NHS-PEG for obtaining the functionalized silver nanoparticles. The authors reported that the PEG-BSA silver nanoparticles were stable in solution for at least five days after the synthesis. Moreover, the combination of indocyanine green-silver nanoparticles resulted in a more stable photothermal effect, reaching temperatures of ≈ 45 °C even after three irradiations with a NIR laser (885 nm, 1.3 W, for 10 min). The in vivo studies performed in B16F10 tumor-bearing mice showed a preferential accumulation in the liver, kidney, and tumors and upon irradiation (885 nm, 0.95 W for 20 min), the tumors' temperature reached 49 °C. This photothermal effect led to the tumors' ablation after four days.

Table 4. Summary of the Platinum/Silver/Zinc-based metallic-polymer nanoconjugates/nanohybrids, their physicochemical properties, and therapeutic applications (N.D.—non disclosed, N.A.—not applicable).

Metal	Morphology	Modification	Size (nm)	Surface Charge (mV)	Loading	In Vitro	In Vivo	Applications	Ref.
Platinum	Spheres	PDA and Folate	≈ 100	N.A.	Indocyanine Green (ICG)	MCF-7	Breast cancer tumor xenograft	PA, FL, PTT ($\lambda_{ex} \approx 700\text{--}800$ nm), and PDT	[136]
		PEG	120	-14.6	DOX	4T1	4T1 tumor-bearing mice	EDT and chemotherapy	[138]
		HA	38 ± 6	-31 ± 1	N.A.	MDA-MB-231 (CD44+) and PC9 (CD44-)	MDA-MB-231 tumor-bearing mice	PI and PTT (N.D.)	[139]
		PEG	119.7	-1.6 ± 0.4	Cisplatin and IR780	4T1	4T1 tumor-bearing mice/Hepatocellular Carcinoma Patient Derived Xenograft	PI, FL, PTT ($\lambda_{ex} = 780$ nm), and chemotherapy	[144]
Silver	Globular irregular shape	BSA and PEG	131.5 ± 2.7	-34.68 ± 0.6	ICG	B16F10 cells	B16F10 tumor-bearing mice	PTT ($\lambda_{ex} \approx 790$ nm)	[143]
	Spheres	Polythiourea and PEG	25–30	N.D.	N.A.	A549	A549 tumor-bearing mice	FL	[145]
		HA	104 ± 6.2	-30	N.A.	4T1	4T1 tumor-bearing mice	FL and RT	[146]
	Dots	FA modified DSPE-PEG ₂₀₀₀	200	-30.84	N.A.	HeLa and A549 cells	HeLa tumor-bearing mice	FL/PA imaging and PTT (Strong absorption in the visible and NIR region)	[147]
Zinc	Spheres	PVP40	≈ 5	-3.6	N.A.	SW480 and HEK293T cells	SW480 tumor-bearing mice	PDT (N.D.)	[133]
		PDA	≈ 175	-21.7	DOX and DNzyme	A549 cells	A549 tumor-bearing mice	FL, PI, GT, PTT (N.D.), and chemotherapy	[148]
		PEG and RGD	112.0 ± 3.2	-14.6 ± 5.2	PTX	4T1 cells	4T1 tumor-bearing mice	MRI, NIRFI, and chemotherapy	[149]
		PEG and PLGA	PLGA-ZnNPc-NP = 141; PLGA-ZnPC-NPs = 152	PLGA-ZnNPc-NPs = 4.8; PLGA-ZnPC-NPs = 5.1	N.A.	MCF-7 cells	DMBA-induced breast cancer-bearing mice	FL and PDT (N.D.)	[150]

Abbreviations—CDT: Chemodynamic Therapy; EDT: Electrodynamical Therapy; FL: Fluorescence Imaging; GT: Gene Therapy; MRI: Magnetic Resonance Imaging; NIRFI: Near Infrared Fluorescence Imaging; PA: Photoacoustic Imaging; PDT: Photodynamic Therapy; PI: Photothermal Imaging; PTT: Photothermal Therapy; RT: Radiotherapy.

3.5. Clinical Trials

Since the 1990s, more than 50 nanomedicines have been approved by the Food and Drug Administration (FDA) and are currently on the market [151]. However, in the last

decade, only a small number of formulations successfully reached the clinic for cancer treatment, a fact that is in part related to the poor pharmacokinetics of the nanomaterials [152]. The latest data indicate that less than 1% of the administered nanoparticles reach the tumor site [153]. Nevertheless, most of the approved nanomedicines are based on liposomes, protein nanoparticles, nano-emulsions, and metal oxide nanoparticles.

Particularly, iron oxide nanoparticles' clinical utility is demonstrated by the FDA approval for application in cancer diagnosis, hyperthermia, and iron deficiency anemia. Among them, it is worth highlighting the various contrast agents based on iron oxide nanoparticles commercially available for MRI, such as Feridex[®], Resovist[®], and Endorem[®]. Moreover, there are more systems under clinical trial, such as Magnablate[®] and Nanotherm[®] (Table 5). The former is an iron oxide nanoparticle developed for magnetohyperthermia applications that underwent a Phase 0 clinical trial (ClinicalTrials.gov Identifier: NCT02033447), with 12 participants, for the thermoablation of prostate cancer (no results are yet available) [154]. In turn, Nanotherm[®] is also based on an aqueous suspension of iron oxide nanoparticles and was already approved by the European Medicines Agency (EMA) for brain tumor treatment [37]. Moreover, recently, a new clinical trial (ClinicalTrials.gov Identifier: NCT05010759; still recruiting) was announced to study the application of Nanotherm[®] in the ablation of prostate carcinoma.

Regarding gold-based nanoparticles, to this date, two promising nanomedicines are currently in clinical trials [151]. AuroLase[®] uses the particles denominated as AuroShell[®], a PEGylated silica-gold nanoshell with ≈ 150 nm in size, for the laser-activated thermal ablation of solid tumors, metastatic lung tumors, and cancer prostatic tissue [151,155]. In the clinical trial (ClinicalTrials.gov Identifier: NCT01679470), a single dose of AuroShell[®] was administered to promote the ablation of primary and/or metastatic lung tumors, still, to this date, no results were posted [156]. There is a second clinical trial (ClinicalTrials.gov Identifier: NCT00848042) involving the utilization of this nanomedicine for the treatment of patients with refractory and/or recurrent head and neck tumors. The patients were subjected to one or more doses of laser irradiation (808 nm) [30,33]. The participants were divided into three groups: (i) five participants, Auroshell[®] dose 4.5 mL kg^{-1} , laser potency 3.5 W; (ii) five participants, Auroshell[®] dose 7.5 mL kg^{-1} , laser potency 4.5 W; (iii) one participant, Auroshell[®] dose 7.5 mL kg^{-1} , laser potency 5 W. However, no data were published to assess the effect on the targeted tumors. In a more recent clinical trial (ClinicalTrials.gov Identifier: NCT02680535), the Auroshell[®] nanoparticles were tested in combination with the MRI/Ultrasound fusion technology to promote the focal ablation of neoplastic prostate tissue. The extension of this clinical trial is still active (ClinicalTrials.gov Identifier: NCT04240639), however no data have been found describing the evolution of the targeted tumors. The NU-0129[®] is another gold-based nanomedicine under clinical trial (ClinicalTrials.gov Identifier: NCT03020017). This nanoparticle is formed by a spherical gold nanoparticle conjugated with siRNA oligonucleotides for targeting BCL2L12 oncogene in glioblastoma multiforme or gliosarcoma treatment applications [151,157]. The early results showed that the NU-0129[®] nanoparticles can cross the blood–brain barrier without unexpected adverse effects, still pending the data regarding antitumoral efficacy [158].

Table 5. Summary of clinical trials comprising metallic-polymer nanoconjugates/nanohybrids (N.A.—not applicable).

Name	Description	Application	Administration Route	Type of Cancer	Clinical Trials Identifier (Phase)	Results	Ref.
Magnablate [®]	Iron oxide nanoparticles	Magnetic Hyperthermia	Intratumoral	Prostate Cancer	NCT02033447 (Early Phase I): Completed	No results yet available	[154]
Nanotherm [®]	Iron oxide nanoparticles	Magnetic Hyperthermia	Intratumoral	Brain tumor	Approved by the EMA in 2010		[37]
			Intratumoral	Prostate Carcinoma	NCT05010759: Still recruiting (Phase not applicable)	No results yet available	N.A.

Table 5. Cont.

Name	Description	Application	Administration Route	Type of Cancer	Clinical Trials Identifier (Phase)	Results	Ref.
AuroLase®	PEGylated silica-gold nanoshell (AuroShell®)	Laser-activated thermal ablation	Intravenous	Metastatic lung tumors	NCT01679470: Phase not applicable	No results yet available	[156]
				Refractory and/or recurrent head and neck tumors	NCT00848042: Phase not applicable	No results yet available	N.A.
				Neoplastic Prostate tissue	NCT02680535 and NCT04240639 (extension of the previous): Phase not applicable	No results yet available	N.A.
NU-0129®	Spherical gold nanoparticle conjugated with siRNA oligonucleotides	Targeting BCL2L12 oncogene	Intravenous	Glioblastoma multiforme or Gliosarcoma Treatment	NCT03020017: Completed	No results provide about the antitumor efficacy	[158]

Abbreviations—EMA: European Medicines Agency; MRI: Magnetic Resonance Imaging; US: Ultrasound Imaging.

4. Conclusions

Metallic-based nanomaterials have been showing promising results in a variety of cancer-related applications, from imaging to the ablation of tumors. Nevertheless, several of these nanomedicines remain in a preclinical stage, an exception being the application of iron oxide-derived nanomaterials in the imaging of tumors.

In this review, the unique set of physicochemical properties that make the metallic nanoparticles highly promising for biomedical applications is described. The high density and X-ray attenuation capacity make these nanomaterials natural contrast agents for conventional imaging techniques such as CT. Moreover, the surface plasmon resonance and/or the magnetism allow the utilization of hyperthermia treatments (e.g., PTT and magneto-hyperthermia). Therefore, the conjugation with natural and/or synthetic polymers can further increase the biological performance of the metallic nanoparticles by enhancing the colloidal stability and blood circulation time as well as conferring additional specificity to the cancer cells. Nevertheless, there remain significant challenges to overcome and effectively translate the metallic-polymer nanoconjugates/nanohybrids to the clinic. Additional studies on the biosafety and long-term fate of these nanomaterials are still missing. Moreover, the optimization and scale-up of the production methods are mandatory to decrease batch-to-batch variability. Furthermore, regulatory agencies should create a comprehensive set of guidelines for the translation of metallic nanoparticles to the clinic.

In summary, the metallic-polymer nanoconjugates/nanohybrids have the potential to support the development of more effective and multifunctional all-in-one nanomedicines, with the capacity to diagnose and treat the tumor as well as monitor in real-time its response to the treatment. Such raw potential of metallic-polymer nanoconjugates/nanohybrids presents an area of opportunity for both researchers and industrial partners (e.g., pharmaceuticals) to develop a new generation of nanomedicines for cancer therapy. Moreover, it is worthwhile to notice that the physicochemical properties of metallic-polymer nanoconjugates/nanohybrids can also be explored to create innovative solutions in the biomedical field, such as biosensors, antimicrobial agents, and tissue regeneration.

Author Contributions: Conceptualization, A.F.M.; methodology, A.Q.F., N.F., C.F.R. and A.F.M.; software, A.Q.F., C.F.R. and A.F.M.; validation, A.F.M. and I.J.C.; formal analysis, A.F.M. and D.d.M.-D.; investigation, A.Q.F., N.F. and C.F.R.; resources, A.F.M., I.J.C. and D.d.M.-D.; data curation, A.Q.F., N.F. and C.F.R.; writing—original draft preparation, A.Q.F., N.F., C.F.R. and A.F.M.; writing—review and editing, A.F.M., I.J.C. and D.d.M.-D.; visualization, I.J.C. and D.d.M.-D.; supervision, A.F.M. and I.J.C.; project administration, I.J.C.; funding acquisition, I.J.C. All authors have read and agreed to the published version of the manuscript.

Funding: This research was funded by the Foundation for Science and Technology (FCT), through funds from the State Budget, and by the European Regional Development Fund (ERDF), under the Portugal 2020 Program, through the Regional Operational Program of the Center (Centro2020), through the Project with the reference UIDB/00709/2020, CENTRO-01-0145-FEDER-028989 and POCI-01-0145-FEDER-031462. The funder had no role in the decision to publish or in the preparation of the manuscript.

Data Availability Statement: The data presented in this article are available at request from the corresponding author.

Acknowledgments: Carolina F. Rodrigues acknowledges her Ph.D. fellowship from FCT (SFRH/BD/144680/2019). Duarte de Melo-Diogo acknowledges FCT for the financial support given through a Junior Researcher contract (2021.00590.CEECIND). Natanael Fernandes acknowledges the individual fellowship from UBI-Banco Santander/Totta. The funders had no role in the decision to publish or in the preparation of the manuscript.

Conflicts of Interest: The authors declare no financial or commercial conflict of interest.

References

1. Aghebati-Maleki, A.; Dolati, S.; Ahmadi, M.; Baghbanzhadeh, A.; Asadi, M.; Fotouhi, A.; Yousefi, M.; Aghebati-Maleki, L. Nanoparticles and cancer therapy: Perspectives for application of nanoparticles in the treatment of cancers. *J. Cell. Physiol.* **2020**, *235*, 1962–1972. [[CrossRef](#)] [[PubMed](#)]
2. Goncalves, A.S.C.; Rodrigues, C.F.; Moreira, A.F.; Correia, I.J. Strategies to improve the photothermal capacity of gold-based nanomedicines. *Acta Biomater.* **2020**, *116*, 105–137. [[CrossRef](#)] [[PubMed](#)]
3. Guimaraes, R.S.; Rodrigues, C.F.; Moreira, A.F.; Correia, I.J. Overview of stimuli-responsive mesoporous organosilica nanocarriers for drug delivery. *Pharmacol. Res.* **2020**, *155*, 104742. [[CrossRef](#)] [[PubMed](#)]
4. Huang, N.; Liu, Y.; Fang, Y.; Zheng, S.; Wu, J.; Wang, M.; Zhong, W.; Shi, M.; Xing, M.; Liao, W. Gold Nanoparticles Induce Tumor Vessel Normalization and Impair Metastasis by Inhibiting Endothelial Smad2/3 Signaling. *ACS Nano* **2020**, *14*, 7940–7958. [[CrossRef](#)]
5. Rodrigues, C.F.; Alves, C.G.; Lima-Sousa, R.; Moreira, A.F.; de Melo-Diogo, D.; Correia, I.J. Inorganic-based drug delivery systems for cancer therapy. In *Advances and Avenues in the Development of Novel Carriers for Bioactives and Biological Agents*; Academic Press: Cambridge, MA, USA, 2020; pp. 283–316.
6. Liu, X.; Yan, B.; Li, Y.; Ma, X.; Jiao, W.; Shi, K.; Zhang, T.; Chen, S.; He, Y.; Liang, X.; et al. Graphene Oxide-Grafted Magnetic Nanorings Mediated Magnetothermodynamic Therapy Favoring Reactive Oxygen Species-Related Immune Response for Enhanced Antitumor Efficacy. *ACS Nano* **2020**, *14*, 1936–1950. [[CrossRef](#)]
7. Li, G.; Zhong, X.; Wang, X.; Gong, F.; Lei, H.; Zhou, Y.; Li, C.; Xiao, Z.; Ren, G.; Zhang, L. Titanium carbide nanosheets with defect structure for photothermal-enhanced sonodynamic therapy. *Bioact. Mater.* **2022**, *8*, 409–419. [[CrossRef](#)]
8. Loh, X.J.; Lee, T.C.; Dou, Q.; Deen, G.R. Utilising inorganic nanocarriers for gene delivery. *Biomater. Sci.* **2016**, *4*, 70–86. [[CrossRef](#)]
9. Liou, G.Y.; Storz, P. Reactive oxygen species in cancer. *Free Radic. Res.* **2010**, *44*, 479–496. [[CrossRef](#)]
10. Tricoli, A.; Righettoni, M.; Teleki, A. Semiconductor gas sensors: Dry synthesis and application. *Angew. Chem. Int. Ed.* **2010**, *49*, 7632–7659. [[CrossRef](#)]
11. Huynh, K.H.; Pham, X.H.; Kim, J.; Lee, S.H.; Chang, H.; Rho, W.Y.; Jun, B.H. Synthesis, Properties, and Biological Applications of Metallic Alloy Nanoparticles. *Int. J. Mol. Sci.* **2020**, *21*, 5174. [[CrossRef](#)]
12. Amendola, V.; Meneghetti, M. Laser ablation synthesis in solution and size manipulation of noble metal nanoparticles. *Phys. Chem. Chem. Phys.* **2009**, *11*, 3805–3821. [[CrossRef](#)]
13. Annamalai, J.; Murugan, P.; Ganapathy, D.; Nallaswamy, D.; Atchudan, R.; Arya, S.; Khosla, A.; Barathi, S.; Sundramoorthy, A.K. Synthesis of various dimensional metal organic frameworks (MOFs) and their hybrid composites for emerging applications—A review. *Chemosphere* **2022**, *298*, 134184. [[CrossRef](#)]
14. Hu, P.; Chen, L.; Kang, X.; Chen, S. Surface Functionalization of Metal Nanoparticles by Conjugated Metal-Ligand Interfacial Bonds: Impacts on Intraparticle Charge Transfer. *Acc. Chem. Res.* **2016**, *49*, 2251–2260. [[CrossRef](#)]
15. Neha, D.; Momin, M.; Khan, T.; Gharat, S.; Ningthoujam, R.S.; Omri, A. Metallic nanoparticles as drug delivery system for the treatment of cancer. *Expert Opin. Drug Deliv.* **2021**, *18*, 1261–1290. [[CrossRef](#)]

16. Xu, J.J.; Zhang, W.C.; Guo, Y.W.; Chen, X.Y.; Zhang, Y.N. Metal nanoparticles as a promising technology in targeted cancer treatment. *Drug Deliv.* **2022**, *29*, 664–678. [[CrossRef](#)]
17. Anselmo, A.C.; Mitragotri, S. A Review of Clinical Translation of Inorganic Nanoparticles. *AAPS J.* **2015**, *17*, 1041–1054. [[CrossRef](#)]
18. Canaparo, R.; Foglietta, F.; Limongi, T.; Serpe, L. Biomedical Applications of Reactive Oxygen Species Generation by Metal Nanoparticles. *Materials* **2020**, *14*, 53. [[CrossRef](#)]
19. Gonzalez-Rubio, G.; Guerrero-Martinez, A.; Liz-Marzan, L.M. Reshaping, Fragmentation, and Assembly of Gold Nanoparticles Assisted by Pulse Lasers. *Acc. Chem. Res.* **2016**, *49*, 678–686. [[CrossRef](#)]
20. Bhatia, S. Natural Polymers vs Synthetic Polymer. In *Natural Polymer Drug Delivery Systems*; Springer: Cham, Switzerland, 2016; pp. 95–118.
21. Aslan, N.; Ceylan, B.; Koç, M.M.; Findik, F. Metallic nanoparticles as X-ray computed tomography (CT) contrast agents: A review. *J. Mol. Struct.* **2020**, *1219*, 128599. [[CrossRef](#)]
22. Liu, Y.; Ai, K.; Lu, L. Nanoparticulate X-ray computed tomography contrast agents: From design validation to in vivo applications. *Acc. Chem. Res.* **2012**, *45*, 1817–1827. [[CrossRef](#)]
23. Cheheltani, R.; Ezzibdeh, R.M.; Chhour, P.; Pulaparathi, K.; Kim, J.; Jurcova, M.; Hsu, J.; Blundell, C.; Litt, H.; Ferrari, V.A.; et al. Tunable, biodegradable gold nanoparticles as contrast agents for computed tomography and photoacoustic imaging. *Biomaterials* **2016**, *102*, 87–97. [[CrossRef](#)] [[PubMed](#)]
24. De La Vega, J.C.; Esquinas, P.L.; Gill, J.K.; Jessa, S.; Gill, B.; Thakur, Y.; Saatchi, K.; Hafeli, U.O. Comparison of Rhenium and Iodine as Contrast Agents in X-ray Imaging. *Contrast Media Mol. Imaging* **2021**, *2021*, 1250360. [[CrossRef](#)] [[PubMed](#)]
25. Berger, M.; Bauser, M.; Frenzel, T.; Hilger, C.S.; Jost, G.; Lauria, S.; Morgenstern, B.; Neis, C.; Pietsch, H.; Sülzle, D.; et al. Hafnium-Based Contrast Agents for X-ray Computed Tomography. *Inorg. Chem.* **2017**, *56*, 5757–5761. [[CrossRef](#)] [[PubMed](#)]
26. Bae, K.T.; McDermott, R.; Gierada, D.S.; Heiken, J.P.; Nolte, M.A.; Takahashi, N.; Hong, C. Gadolinium-enhanced computed tomography angiography in multi-detector row computed tomography. *Acad. Radiol.* **2004**, *11*, 61–68. [[CrossRef](#)]
27. Werts, M.H.V.; Allix, F.; Francois, O.; Frochot, C.; Griscom, L.; Le Pioufle, B.; Loumagne, M.; Midelet, J. Manipulation and Optical Detection of Colloidal Functional Plasmonic Nanostructures in Microfluidic Systems. *IEEE J. Sel. Top. Quantum Electron.* **2014**, *20*, 102–114.
28. Wang, L.; Hasanzadeh Kafshgari, M.; Meunier, M. Optical Properties and Applications of Plasmonic-Metal Nanoparticles. *Adv. Funct. Mater.* **2020**, *30*, 2005400. [[CrossRef](#)]
29. Noguez, C. Surface Plasmons on Metal Nanoparticles: The Influence of Shape and Physical Environment. *J. Phys. Chem. C* **2007**, *111*, 3806–3819. [[CrossRef](#)]
30. Liz-Marzán, L.M. Tailoring Surface Plasmons through the Morphology and Assembly of Metal Nanoparticles. *Langmuir* **2006**, *22*, 32–41. [[CrossRef](#)]
31. Liang, J.; Liu, H.; Yu, J.; Zhou, L.; Zhu, J. Plasmon-enhanced solar vapor generation. *Nanophotonics* **2019**, *8*, 771–786. [[CrossRef](#)]
32. Jeong, Y.; Kook, Y.M.; Lee, K.; Koh, W.G. Metal enhanced fluorescence (MEF) for biosensors: General approaches and a review of recent developments. *Biosens. Bioelectron.* **2018**, *111*, 102–116. [[CrossRef](#)]
33. Lin, Q.; Jia, M.; Fu, Y.; Li, B.; Dong, Z.; Niu, X.; You, Z. Upper-Critical-Solution-Temperature Polymer Modified Gold Nanorods for Laser Controlled Drug Release and Enhanced Anti-Tumour Therapy. *Front. Pharm.* **2021**, *12*, 738630. [[CrossRef](#)]
34. de Melo-Diogo, D.; Pais-Silva, C.; Dias, D.R.; Moreira, A.F.; Correia, I.J. Strategies to Improve Cancer Photothermal Therapy Mediated by Nanomaterials. *Adv. Healthc. Mater.* **2017**, *6*, 1700073. [[CrossRef](#)]
35. Bettaieb, A.; Wrzal, K.P.; Averill-Bates, D.A. Hyperthermia: Cancer Treatment and Beyond. *Cancer Treat. Conv. Innov. Approaches* **2013**, 257–283. [[CrossRef](#)]
36. Zhang, Y.; Zhan, X.; Xiong, J.; Peng, S.; Huang, W.; Joshi, R.; Cai, Y.; Liu, Y.; Li, R.; Yuan, K.; et al. Temperature-dependent cell death patterns induced by functionalized gold nanoparticle photothermal therapy in melanoma cells. *Sci. Rep.* **2018**, *8*, 8720. [[CrossRef](#)]
37. Fernandes, N.; Rodrigues, C.F.; Moreira, A.F.; Correia, I.J. Overview of the application of inorganic nanomaterials in cancer photothermal therapy. *Biomater. Sci.* **2020**, *8*, 2990–3020. [[CrossRef](#)]
38. Xing, Y.; Cai, Z.; Xu, M.; Ju, W.; Luo, X.; Hu, Y.; Liu, X.; Kang, T.; Wu, P.; Cai, C.; et al. Raman observation of a molecular signaling pathway of apoptotic cells induced by photothermal therapy. *Chem. Sci.* **2019**, *10*, 10900–10910. [[CrossRef](#)]
39. Jiang, Z.; Li, T.; Cheng, H.; Zhang, F.; Yang, X.; Wang, S.; Zhou, J.; Ding, Y. Nanomedicine potentiates mild photothermal therapy for tumor ablation. *Asian J. Pharm. Sci.* **2021**, *16*, 738–761. [[CrossRef](#)]
40. Rudakov, G.A.; Tsiberkin, K.B.; Ponomarev, R.S.; Henner, V.K.; Ziolkowska, D.A.; Jasinski, J.B.; Sumanasekera, G. Magnetic properties of transition metal nanoparticles enclosed in carbon nanocages. *J. Magn. Magn. Mater.* **2019**, *472*, 34–39. [[CrossRef](#)]
41. Soheilian, R.; Choi, Y.S.; David, A.E.; Abdi, H.; Maloney, C.E.; Erb, R.M. Toward Accumulation of Magnetic Nanoparticles into Tissues of Small Porosity. *Langmuir* **2015**, *31*, 8267–8274. [[CrossRef](#)]
42. Guo, X.; Li, W.; Luo, L.; Wang, Z.; Li, Q.; Kong, F.; Zhang, H.; Yang, J.; Zhu, C.; Du, Y.; et al. External Magnetic Field-Enhanced Chemo-Photothermal Combination Tumor Therapy via Iron Oxide Nanoparticles. *ACS Appl. Mater. Interfaces* **2017**, *9*, 16581–16593. [[CrossRef](#)]
43. Farzin, A.; Etesami, S.A.; Quint, J.; Memic, A.; Tamayol, A. Magnetic Nanoparticles in Cancer Therapy and Diagnosis. *Adv. Healthc. Mater.* **2020**, *9*, e1901058. [[CrossRef](#)] [[PubMed](#)]

44. Sengul, A.B.; Asmatulu, E. Toxicity of metal and metal oxide nanoparticles: A review. *Environ. Chem. Lett.* **2020**, *18*, 1659–1683. [[CrossRef](#)]
45. Wu, H.; Yin, J.J.; Wamer, W.G.; Zeng, M.; Lo, Y.M. Reactive oxygen species-related activities of nano-iron metal and nano-iron oxides. *J. Food Drug Anal.* **2014**, *22*, 86–94. [[CrossRef](#)] [[PubMed](#)]
46. Yuan, P.; Ding, X.; Yang, Y.Y.; Xu, Q.-H. Metal Nanoparticles for Diagnosis and Therapy of Bacterial Infection. *Adv. Healthc. Mater.* **2018**, *7*, 1701392. [[CrossRef](#)]
47. Juarranz, Á.; Jaén, P.; Sanz-Rodríguez, F.; Cuevas, J.; González, S. Photodynamic therapy of cancer. Basic principles and applications. *Clin. Transl. Oncol.* **2008**, *10*, 148–154. [[CrossRef](#)]
48. Wilson, B.C. Photodynamic Therapy for Cancer: Principles. *Can. J. Gastroenterol.* **2002**, *16*, 743109. [[CrossRef](#)]
49. Vinković Vrček, I.; Pavičić, I.; Crnković, T.; Jurašin, D.; Babič, M.; Horák, D.; Lovric, M.; Ferhatovic, L.; Curlin, M.; Gajovic, S. Does surface coating of metallic nanoparticles modulate their interference with in vitro assays? *RSC Adv.* **2015**, *5*, 70787–70807. [[CrossRef](#)]
50. Rajendran, K.; Pujari, L.; Krishnamoorthy, M.; Sen, S.; Dharmaraj, D.; Karuppiah, K.; Ethiraj, K. Toxicological evaluation of biosynthesised hematite nanoparticles in vivo. *Colloids Surf. B Biointerfaces* **2021**, *198*, 111475. [[CrossRef](#)]
51. García-Álvarez, R.; Hadjidemetriou, M.; Sánchez-Iglesias, A.; Liz-Marzán, L.M.; Kostarelos, K. In vivo formation of protein corona on gold nanoparticles. The effect of their size and shape. *Nanoscale* **2018**, *10*, 1256–1264. [[CrossRef](#)]
52. Thambiraj, S.; Vijayalakshmi, R.; Ravi Shankaran, D. An effective strategy for development of docetaxel encapsulated gold nanoformulations for treatment of prostate cancer. *Sci. Rep.* **2021**, *11*, 2808. [[CrossRef](#)]
53. Hada, A.M.; Craciun, A.M.; Focsan, M.; Borlan, R.; Soritau, O.; Todea, M.; Astilean, S. Folic acid functionalized gold nanoclusters for enabling targeted fluorescence imaging of human ovarian cancer cells. *Talanta* **2021**, *225*, 121960. [[CrossRef](#)]
54. Kim, H.S.; Lee, S.J.; Lee, D.Y. Milk protein-shelled gold nanoparticles with gastrointestinally active absorption for aurotherapy to brain tumor. *Bioact. Mater.* **2022**, *8*, 35–48. [[CrossRef](#)]
55. Mapanao, A.K.; Santi, M.; Voliani, V. Combined chemo-photothermal treatment of three-dimensional head and neck squamous cell carcinomas by gold nano-architectures. *J. Colloid Interface Sci.* **2021**, *582*, 1003–1011. [[CrossRef](#)]
56. You, Y.H.; Lin, Y.F.; Nirosha, B.; Chang, H.T.; Huang, Y.F. Polydopamine-coated gold nanostar for combined antitumor and antiangiogenic therapy in multidrug-resistant breast cancer. *Nanotheranostics* **2019**, *3*, 266–283. [[CrossRef](#)]
57. Sheng, Y.; Liu, C.; Yuan, Y.; Tao, X.; Yang, F.; Shan, X.; Zhou, H.; Xu, F. Long-circulating polymeric nanoparticles bearing a combinatorial coating of PEG and water-soluble chitosan. *Biomaterials* **2009**, *30*, 2340–2348. [[CrossRef](#)]
58. Li, B.; Xie, J.; Yuan, Z.; Jain, P.; Lin, X.; Wu, K.; Jiang, S. Mitigation of Inflammatory Immune Responses with Hydrophilic Nanoparticles. *Angew. Chem. Int. Ed.* **2018**, *57*, 4527–4531. [[CrossRef](#)]
59. Lowe, S.; O'Brien-Simpson, N.M.; Connal, L.A. Antibiofouling polymer interfaces: Poly(ethylene glycol) and other promising candidates. *Polym. Chem.* **2015**, *6*, 198–212. [[CrossRef](#)]
60. Yu, Y.; Luan, Y.; Dai, W. Dynamic process, mechanisms, influencing factors and study methods of protein corona formation. *Int. J. Biol. Macromol.* **2022**, *205*, 731–739. [[CrossRef](#)]
61. Feng, W.; Zhu, S.; Ishihara, K.; Brash, J.L. Protein resistant surfaces: Comparison of acrylate graft polymers bearing oligo-ethylene oxide and phosphorylcholine side chains. *Biointerphases* **2006**, *1*, 50. [[CrossRef](#)]
62. He, M.; Gao, K.; Zhou, L.; Jiao, Z.; Wu, M.; Cao, J.; You, X.; Cai, Z.; Su, Y.; Jiang, Z. Zwitterionic materials for antifouling membrane surface construction. *Acta Biomater.* **2016**, *40*, 142–152. [[CrossRef](#)]
63. Zhang, Y.; Liu, Y.; Ren, B.; Zhang, D.; Xie, S.; Chang, Y.; Yang, J.; Wu, J.; Xu, L.; Zheng, J. Fundamentals and applications of zwitterionic antifouling polymers. *J. Phys. D Appl. Phys.* **2019**, *52*, 403001. [[CrossRef](#)]
64. Liu, X.; Li, H.; Chen, Y.; Jin, Q.; Ren, K.; Ji, J. Mixed-Charge Nanoparticles for Long Circulation, Low Reticuloendothelial System Clearance, and High Tumor Accumulation. *Adv. Healthc. Mater.* **2014**, *3*, 1439–1447. [[CrossRef](#)]
65. Wu, L.; Lin, B.; Yang, H.; Chen, J.; Mao, Z.; Wang, W.; Gao, C. Enzyme-responsive multifunctional peptide coating of gold nanorods improves tumor targeting and photothermal therapy efficacy. *Acta Biomater.* **2019**, *86*, 363–372. [[CrossRef](#)] [[PubMed](#)]
66. Li, W.; Cao, Z.; Yu, L.; Huang, Q.; Zhu, D.; Lu, C.; Lu, A.; Liu, Y. Hierarchical drug release designed Au @PDA-PEG-MTX NPs for targeted delivery to breast cancer with combined photothermal-chemotherapy. *J. Nanobiotechnol.* **2021**, *19*, 143. [[CrossRef](#)] [[PubMed](#)]
67. Sathiyaseelan, A.; Saravanakumar, K.; Mariadoss, A.V.A.; Wang, M.H. pH-controlled nucleolin targeted release of dual drug from chitosan-gold based aptamer functionalized nano drug delivery system for improved glioblastoma treatment. *Carbohydr. Polym.* **2021**, *262*, 117907. [[CrossRef](#)] [[PubMed](#)]
68. Feng, Y.; Cheng, Y.; Chang, Y.; Jian, H.; Zheng, R.; Wu, X.; Xu, K.; Wang, L.; Ma, X.; Li, X.; et al. Time-staggered delivery of erlotinib and doxorubicin by gold nanocages with two smart polymers for reprogrammable release and synergistic with photothermal therapy. *Biomaterials* **2019**, *217*, 119327. [[CrossRef](#)]
69. Wang, N.; Shi, J.; Wu, C.; Chu, W.; Tao, W.; Li, W.; Yuan, X. Design of DOX-GNRs-PNIPAM@PEG-PLA Micelle With Temperature and Light Dual-Function for Potent Melanoma Therapy. *Front. Chem.* **2020**, *8*, 599740. [[CrossRef](#)]
70. Li, D.; Zhang, R.; Liu, G.; Kang, Y.; Wu, J. Redox-Responsive Self-Assembled Nanoparticles for Cancer Therapy. *Adv. Healthc. Mater.* **2020**, *9*, 2000605. [[CrossRef](#)]
71. Shi, Y.; van der Meel, R.; Chen, X.; Lammers, T. The EPR effect and beyond: Strategies to improve tumor targeting and cancer nanomedicine treatment efficacy. *Theranostics* **2020**, *10*, 7921–7924. [[CrossRef](#)]

72. Acharya, S.; Sahoo, S.K. PLGA nanoparticles containing various anticancer agents and tumour delivery by EPR effect. *Adv. Drug Deliv. Rev.* **2011**, *63*, 170–183. [[CrossRef](#)]
73. Yucel, O.; Sengelen, A.; Emik, S.; Onay-Ucar, E.; Arda, N.; Gurdag, G. Folic acid-modified methotrexate-conjugated gold nanoparticles as nano-sized trojans for drug delivery to folate receptor-positive cancer cells. *Nanotechnology* **2020**, *31*, 355101. [[CrossRef](#)]
74. Mulens-Arias, V.; Nicolas-Boluda, A.; Pinto, A.; Balfourier, A.; Carn, F.; Silva, A.K.A.; Pocard, M.; Gazeau, F. Tumor-Selective Immune-Active Mild Hyperthermia Associated with Chemotherapy in Colon Peritoneal Metastasis by Photoactivation of Fluorouracil-Gold Nanoparticle Complexes. *ACS Nano* **2021**, *15*, 3330–3348. [[CrossRef](#)]
75. Guo, J.; Rahme, K.; He, Y.; Li, L.L.; Holmes, J.D.; O'Driscoll, C.M. Gold nanoparticles enlighten the future of cancer theranostics. *Int. J. Nanomed.* **2017**, *12*, 6131–6152. [[CrossRef](#)]
76. Cole, L.E.; Ross, R.D.; Tilley, J.M.R.; Vargo-Gogola, T.; Roeder, R.K. Gold nanoparticles as contrast agents in x-ray imaging and computed tomography. *Nanomedicine* **2015**, *10*, 321–341. [[CrossRef](#)]
77. Xi, D.; Dong, S.; Meng, X.; Lu, Q.; Meng, L.; Ye, J. Gold nanoparticles as computerized tomography (CT) contrast agents. *RSC Adv.* **2012**, *2*, 12515. [[CrossRef](#)]
78. Capek, I. Polymer decorated gold nanoparticles in nanomedicine conjugates. *Adv. Colloid Interface Sci.* **2017**, *249*, 386–399. [[CrossRef](#)]
79. Guo, C.; Hall, G.N.; Addison, J.B.; Yarger, J.L. Gold nanoparticle-doped silk film as biocompatible SERS substrate. *RSC Adv.* **2015**, *5*, 1937–1942. [[CrossRef](#)]
80. Fernandes, N.; Rodrigues, C.F.; de Melo-Diogo, D.; Correia, I.J.; Moreira, A.F. Optimization of the GSH-Mediated Formation of Mesoporous Silica-Coated Gold Nanoclusters for NIR Light-Triggered Photothermal Applications. *Nanomaterials* **2021**, *11*, 1946. [[CrossRef](#)]
81. Fernandes, J.; Kang, S. Numerical Study on the Surface Plasmon Resonance Tunability of Spherical and Non-Spherical Core-Shell Dimer Nanostructures. *Nanomaterials* **2021**, *11*, 1728. [[CrossRef](#)]
82. Xu, H.; Käll, M. Modeling the optical response of nanoparticle-based surface plasmon resonance sensors. *Sens. Actuators B Chem.* **2002**, *87*, 244–249. [[CrossRef](#)]
83. Bouhelier, A.; Bachelot, R.; Lerondel, G.; Kostcheev, S.; Royer, P.; Wiederrecht, G.P. Surface plasmon characteristics of tunable photoluminescence in single gold nanorods. *Phys. Rev. Lett* **2005**, *95*, 267405. [[CrossRef](#)] [[PubMed](#)]
84. Chandrasekaran, R.; Lee, A.S.W.; Yap, L.W.; Jans, D.A.; Wagstaff, K.M.; Cheng, W. Tumor cell-specific photothermal killing by SELEX-derived DNA aptamer-targeted gold nanorods. *Nanoscale* **2016**, *8*, 187–196. [[CrossRef](#)] [[PubMed](#)]
85. Shi, W.; Casas, J.; Venkataramasubramani, M.; Tang, L. Synthesis and Characterization of Gold Nanoparticles with Plasmon Absorbance Wavelength Tunable from Visible to Near Infrared Region. *ISRN Nanomater.* **2012**, *2012*, 659043. [[CrossRef](#)]
86. Jacinto, T.A.; Rodrigues, C.F.; Moreira, A.F.; Miguel, S.P.; Costa, E.C.; Ferreira, P.; Correia, I.J. Hyaluronic acid and vitamin E polyethylene glycol succinate functionalized gold-core silica shell nanorods for cancer targeted photothermal therapy. *Colloids Surf. B Biointerfaces* **2020**, *188*, 110778. [[CrossRef](#)]
87. F Rodrigues, C.; Fernandes, N.; de Melo-Diogo, D.; Ferreira, P.; J Correia, I.; F Moreira, A. HA/PEI-coated acridine orange-loaded gold-core silica shell nanorods for cancer-targeted photothermal and chemotherapy. *Nanomedicine* **2021**, *16*, 2569–2586. [[CrossRef](#)]
88. Pan, Y.; Ma, X.; Liu, C.; Xing, J.; Zhou, S.; Parshad, B.; Schwerdtle, T.; Li, W.; Wu, A.; Haag, R. Retinoic Acid-Loaded Dendritic Polyglycerol-Conjugated Gold Nanostars for Targeted Photothermal Therapy in Breast Cancer Stem Cells. *ACS Nano* **2021**, *15*, 15069–15084. [[CrossRef](#)]
89. Tan, H.; Hou, N.; Liu, Y.; Liu, B.; Cao, W.; Zheng, D.; Li, W.; Liu, Y.; Xu, B.; Wang, Z.; et al. CD133 antibody targeted delivery of gold nanostars loading IR820 and docetaxel for multimodal imaging and near-infrared photodynamic/photothermal/chemotherapy against castration resistant prostate cancer. *Nanomedicine* **2020**, *27*, 102192. [[CrossRef](#)]
90. Cheng, Y.; Bao, D.; Chen, X.; Wu, Y.; Wei, Y.; Wu, Z.; Li, F.; Piao, J.G. Microwave-triggered/HSP-targeted gold nano-system for triple-negative breast cancer photothermal therapy. *Int. J. Pharm.* **2021**, *593*, 120162. [[CrossRef](#)]
91. Peng, C.; Zheng, L.; Chen, Q.; Shen, M.; Guo, R.; Wang, H.; Cao, X.; Zhang, G.; Shi, X. PEGylated dendrimer-entrapped gold nanoparticles for in vivo blood pool and tumor imaging by computed tomography. *Biomaterials* **2012**, *33*, 1107–1119. [[CrossRef](#)]
92. Gu, W.; Zhang, Q.; Zhang, T.; Li, Y.; Xiang, J.; Peng, R.; Liu, J. Hybrid polymeric nano-capsules loaded with gold nanoclusters and indocyanine green for dual-modal imaging and photothermal therapy. *J. Mater. Chem. B* **2016**, *4*, 910–919. [[CrossRef](#)]
93. Alkhayal, A.; Fathima, A.; Alhasan, A.H.; Alsharaeh, E.H. PEG Coated Fe₃O₄/RGO Nano-Cube-Like Structures for Cancer Therapy via Magnetic Hyperthermia. *Nanomaterials* **2021**, *11*, 2398. [[CrossRef](#)]
94. Ebrahiminezhad, A.; Zare-Hoseinabadi, A.; Sarmah, A.K.; Taghizadeh, S.; Ghasemi, Y.; Berenjjan, A. Plant-Mediated Synthesis and Applications of Iron Nanoparticles. *Mol. Biotechnol.* **2018**, *60*, 154–168. [[CrossRef](#)]
95. Zhi, D.; Yang, T.; Yang, J.; Fu, S.; Zhang, S. Targeting strategies for superparamagnetic iron oxide nanoparticles in cancer therapy. *Acta Biomater.* **2020**, *102*, 13–34. [[CrossRef](#)]
96. Palanisamy, S.; Wang, Y.M. Superparamagnetic iron oxide nanoparticulate system: Synthesis, targeting, drug delivery and therapy in cancer. *Dalton Trans.* **2019**, *48*, 9490–9515. [[CrossRef](#)]
97. Habra, K.; McArdle, S.E.B.; Morris, R.H.; Cave, G.W.V. Synthesis and Functionalisation of Superparamagnetic Nano-Rods towards the Treatment of Glioblastoma Brain Tumours. *Nanomaterials* **2021**, *11*, 2157. [[CrossRef](#)]

98. Vangijzegem, T.; Stanicki, D.; Laurent, S. Magnetic iron oxide nanoparticles for drug delivery: Applications and characteristics. *Expert Opin. Drug Deliv.* **2019**, *16*, 69–78. [[CrossRef](#)]
99. Liu, J.F.; Jang, B.; Issadore, D.; Tsourkas, A. Use of magnetic fields and nanoparticles to trigger drug release and improve tumor targeting. *WIREs Nanomed. Nanobiotechnol.* **2019**, *11*, e1571. [[CrossRef](#)]
100. Shah, R.R.; Davis, T.P.; Glover, A.L.; Nikles, D.E.; Brazel, C.S. Impact of magnetic field parameters and iron oxide nanoparticle properties on heat generation for use in magnetic hyperthermia. *J. Magn. Magn. Mater.* **2015**, *387*, 96–106. [[CrossRef](#)]
101. Obaidat, I.M.; Issa, B.; Haik, Y. Magnetic Properties of Magnetic Nanoparticles for Efficient Hyperthermia. *Nanomaterials* **2015**, *5*, 63–89. [[CrossRef](#)]
102. Boyer, C.; Whittaker, M.R.; Bulmus, V.; Liu, J.; Davis, T.P. The design and utility of polymer-stabilized iron-oxide nanoparticles for nanomedicine applications. *NPG Asia Mater.* **2010**, *2*, 23–30. [[CrossRef](#)]
103. Xu, X.; Zhou, X.; Xiao, B.; Xu, H.; Hu, D.; Qian, Y.; Hu, H.; Zhou, Z.; Liu, X.; Gao, J.; et al. Glutathione-Responsive Magnetic Nanoparticles for Highly Sensitive Diagnosis of Liver Metastases. *Nano Lett.* **2021**, *21*, 2199–2206. [[CrossRef](#)]
104. Xiao, Z.; You, Y.; Liu, Y.; He, L.; Zhang, D.; Cheng, Q.; Wang, D.; Chen, T.; Shi, C.; Luo, L. NIR-Triggered Blasting Nanovesicles for Targeted Multimodal Image-Guided Synergistic Cancer Photothermal and Chemotherapy. *ACS Appl. Mater. Interfaces* **2021**, *13*, 35376–35388. [[CrossRef](#)] [[PubMed](#)]
105. Chen, L.; Wu, Y.; Wu, H.; Li, J.; Xie, J.; Zang, F.; Ma, M.; Gu, N.; Zhang, Y. Magnetic targeting combined with active targeting of dual-ligand iron oxide nanoprobe to promote the penetration depth in tumors for effective magnetic resonance imaging and hyperthermia. *Acta Biomater.* **2019**, *96*, 491–504. [[CrossRef](#)] [[PubMed](#)]
106. Zhang, Y.; Hu, H.; Tang, W.; Zhang, Q.; Li, M.; Jin, H.; Huang, Z.; Cui, Z.; Xu, J.; Wang, K.; et al. A multifunctional magnetic nanosystem based on “two strikes” effect for synergistic anticancer therapy in triple-negative breast cancer. *J. Control. Release* **2020**, *322*, 401–415. [[CrossRef](#)] [[PubMed](#)]
107. Zheng, D.; Wan, C.; Yang, H.; Xu, L.; Dong, Q.; Du, C.; Du, J.; Li, F. Her2-Targeted Multifunctional Nano-Theranostic Platform Mediates Tumor Microenvironment Remodeling and Immune Activation for Breast Cancer Treatment. *Int. J. Nanomed.* **2020**, *15*, 10007–10028. [[CrossRef](#)]
108. He, Y.; Wang, M.; Fu, M.; Yuan, X.; Luo, Y.; Qiao, B.; Cao, J.; Wang, Z.; Hao, L.; Yuan, G. Iron(II) phthalocyanine Loaded and AS1411 Aptamer Targeting Nanoparticles: A Nanocomplex for Dual Modal Imaging and Photothermal Therapy of Breast Cancer. *Int. J. Nanomed.* **2020**, *15*, 5927–5949. [[CrossRef](#)]
109. Ding, X.; Jiang, W.; Dong, L.; Hong, C.; Luo, Z.; Hu, Y.; Cai, K. Redox-responsive magnetic nanovectors self-assembled from amphiphilic polymer and iron oxide nanoparticles for a remotely targeted delivery of paclitaxel. *J. Mater. Chem. B* **2021**, *9*, 6037–6043. [[CrossRef](#)]
110. Lin, C.H.; Chen, Y.C.; Huang, P.I. Preparation of Multifunctional Dopamine-Coated Zerovalent Iron/Reduced Graphene Oxide for Targeted Phototheragnosis in Breast Cancer. *Nanomaterials* **2020**, *10*, 1957. [[CrossRef](#)]
111. Yun, B.; Zhu, H.; Yuan, J.; Sun, Q.; Li, Z. Synthesis, modification and bioapplications of nanoscale copper chalcogenides. *J. Mater. Chem. B* **2020**, *8*, 4778–4812. [[CrossRef](#)]
112. Zhou, M.; Tian, M.; Li, C. Copper-Based Nanomaterials for Cancer Imaging and Therapy. *Bioconjugate Chem.* **2016**, *27*, 1188–1199. [[CrossRef](#)]
113. Rubilar, O.; Rai, M.; Tortella, G.; Diez, M.C.; Seabra, A.B.; Duran, N. Biogenic nanoparticles: Copper, copper oxides, copper sulphides, complex copper nanostructures and their applications. *Biotechnol. Lett.* **2013**, *35*, 1365–1375. [[CrossRef](#)]
114. Tian, H.; Zhang, M.; Jin, G.; Jiang, Y.; Luan, Y. Cu-MOF chemodynamic nanoplatfrom via modulating glutathione and H₂O₂ in tumor microenvironment for amplified cancer therapy. *J. Colloid Interface Sci.* **2021**, *587*, 358–366. [[CrossRef](#)]
115. Wang, S.; Riedinger, A.; Li, H.; Fu, C.; Liu, H.; Li, L.; Liu, T.; Tan, L.; Barthel, M.J.; Pugliese, G.; et al. Plasmonic Copper Sulfide Nanocrystals Exhibiting Near-Infrared Photothermal and Photodynamic Therapeutic Effects. *ACS Nano* **2015**, *9*, 1788–1800. [[CrossRef](#)]
116. Egorova, K.S.; Ananikov, V.P. Which Metals are Green for Catalysis? Comparison of the Toxicities of Ni, Cu, Fe, Pd, Pt, Rh, and Au Salts. *Angew. Chem. Int. Ed.* **2016**, *55*, 12150–12162. [[CrossRef](#)]
117. Letelier, M.E.; Sánchez-Jofré, S.; Peredo-Silva, L.; Cortés-Troncoso, J.; Aracena-Parks, P. Mechanisms underlying iron and copper ions toxicity in biological systems: Pro-oxidant activity and protein-binding effects. *Chem. Biol. Interact.* **2010**, *188*, 220–227. [[CrossRef](#)]
118. Li, W.; Zamani, R.; Gil, P.R.; Pelaz, B.; Ibáñez, M.; Cadavid, D.; Shavel, A.; Alvarez-Puebla, R.A.; Parak, W.J.; Arbiol, J.; et al. CuTe Nanocrystals: Shape and Size Control, Plasmonic Properties, and Use as SERS Probes and Photothermal Agents. *J. Am. Chem. Soc.* **2013**, *135*, 7098–7101. [[CrossRef](#)]
119. Li, L.; Rashidi, L.H.; Yao, M.; Ma, L.; Chen, L.; Zhang, J.; Zhang, Y.; Chen, W. CuS nanoagents for photodynamic and photothermal therapies: Phenomena and possible mechanisms. *Photodiagn. Photodyn.* **2017**, *19*, 5–14. [[CrossRef](#)]
120. Shi, H.; Yan, R.; Wu, L.; Sun, Y.; Liu, S.; Zhou, Z.; He, J.; Ye, D. Tumor-targeting CuS nanoparticles for multimodal imaging and guided photothermal therapy of lymph node metastasis. *Acta Biomater.* **2018**, *72*, 256–265. [[CrossRef](#)]
121. Xu, J.; Shi, R.; Chen, G.; Dong, S.; Yang, P.; Zhang, Z.; Niu, N.; Gai, S.; He, F.; Fu, Y.; et al. All-in-One Theranostic Nanomedicine with Ultrabright Second Near-Infrared Emission for Tumor-Modulated Bioimaging and Chemodynamic/Photodynamic Therapy. *ACS Nano* **2020**, *14*, 9613–9625. [[CrossRef](#)]

122. Liang, S.; Deng, X.; Chang, Y.; Sun, C.; Shao, S.; Xie, Z.; Xiao, X.; Ma, P.; Zhang, H.; Cheng, Z.; et al. Intelligent Hollow Pt-CuS Janus Architecture for Synergistic Catalysis-Enhanced Sonodynamic and Photothermal Cancer Therapy. *Nano Lett.* **2019**, *19*, 4134–4145. [[CrossRef](#)]
123. Poudel, K.; Thapa, R.K.; Gautam, M.; Ou, W.; Soe, Z.C.; Gupta, B.; Ruttala, H.B.; Thuy, H.N.; Dai, P.C.; Jeong, J.-H.; et al. Multifaceted NIR-responsive polymer-peptide-enveloped drug-loaded copper sulfide nanoplatform for chemo-phototherapy against highly tumorigenic prostate cancer. *Nanomedicine* **2019**, *21*, 102042. [[CrossRef](#)] [[PubMed](#)]
124. Maor, I.; Asadi, S.; Korganbayev, S.; Dahis, D.; Shamay, Y.; Schena, E.; Azhari, H.; Saccomandi, P.; Weitz, I.S. Laser-induced thermal response and controlled release of copper oxide nanoparticles from multifunctional polymeric nanocarriers. *Sci. Technol. Adv. Mater.* **2021**, *22*, 218–233. [[CrossRef](#)] [[PubMed](#)]
125. Xu, R.; Zhang, K.; Liang, J.; Gao, F.; Li, J.; Guan, F. Hyaluronic acid/polyethyleneimine nanoparticles loaded with copper ion and disulfiram for esophageal cancer. *Carbohydr. Polym.* **2021**, *261*, 117846. [[CrossRef](#)] [[PubMed](#)]
126. Wu, Z.; Zhang, P.; Wang, P.; Wang, Z.; Luo, X. Using copper sulfide nanoparticles as cross-linkers of tumor microenvironment responsive polymer micelles for cancer synergistic photo-chemotherapy. *Nanoscale* **2021**, *13*, 3723–3736. [[CrossRef](#)]
127. Xiao, Z.; Zuo, W.; Chen, L.; Wu, L.; Liu, N.; Liu, J.; Jin, Q.; Zhao, Y.; Zhu, X. H₂O₂ Self-Supplying and GSH-Depleting Nanoplatform for Chemodynamic Therapy Synergetic Photothermal/Chemotherapy. *ACS Appl. Mater. Interfaces* **2021**, *13*, 43925–43936. [[CrossRef](#)]
128. Cai, X.; Xie, Z.; Ding, B.; Shao, S.; Liang, S.; Pang, M.; Lin, J. Monodispersed Copper(I)-Based Nano Metal-Organic Framework as a Biodegradable Drug Carrier with Enhanced Photodynamic Therapy Efficacy. *Adv. Sci.* **2019**, *6*, 1900848. [[CrossRef](#)]
129. Fang, X.L.; Akrofi, R.; Yang, H.; Chen, Q.Y. The NIR inspired nano-CuSMn(II) composites for lactate and glycolysis attenuation. *Colloids Surf. B Biointerfaces* **2019**, *181*, 728–733. [[CrossRef](#)]
130. Yu, X.; Yu, J.; Cheng, B.; Huang, B. One-Pot Template-Free Synthesis of Monodisperse Zinc Sulfide Hollow Spheres and Their Photocatalytic Properties. *Chem. A Eur. J.* **2009**, *15*, 6731–6739. [[CrossRef](#)]
131. Wang, C.-C.; Wang, S.; Xia, Q.; He, W.; Yin, J.-J.; Fu, P.P.; Li, J.-H. Phototoxicity of Zinc Oxide Nanoparticles in HaCaT Keratinocytes-Generation of Oxidative DNA Damage During UVA and Visible Light Irradiation. *J. Nanosci. Nanotechnol.* **2013**, *13*, 3880–3888. [[CrossRef](#)]
132. Akhtar, M.J.; Ahamed, M.; Kumar, S.; Khan, M.M.; Ahmad, J.; Alrokayan, S.A. Zinc oxide nanoparticles selectively induce apoptosis in human cancer cells through reactive oxygen species. *Int. J. Nanomed.* **2012**, *7*, 845–857.
133. Song, T.; Qu, Y.; Ren, Z.; Yu, S.; Sun, M.; Yu, X.; Yu, X. Synthesis and Characterization of Polyvinylpyrrolidone-Modified ZnO Quantum Dots and Their In Vitro Photodynamic Tumor Suppressive Action. *Int. J. Mol. Sci.* **2021**, *22*, 8106. [[CrossRef](#)]
134. Riddell, I.A.; Lippard, S.J. Cisplatin and Oxaliplatin: Our Current Understanding of Their Actions. *Met. Ions Life Sci.* **2018**, *18*, 1–42.
135. Asharani, P.V.; Xinyi, N.; Hande, M.P.; Valiyaveetil, S. DNA damage and p53-mediated growth arrest in human cells treated with platinum nanoparticles. *Nanomedicine* **2009**, *5*, 51–64. [[CrossRef](#)]
136. Cao, H.; Yang, Y.; Liang, M.; Ma, Y.; Sun, N.; Gao, X.; Li, J. Pt@polydopamine nanoparticles as nanozymes for enhanced photodynamic and photothermal therapy. *Chem. Commun.* **2021**, *57*, 255–258. [[CrossRef](#)]
137. Pedone, D.; Moglianetti, M.; De Luca, E.; Bardi, G.; Pompa, P.P. Platinum nanoparticles in nanobiomedicine. *Chem. Soc. Rev.* **2017**, *46*, 4951–4975. [[CrossRef](#)]
138. Chen, T.; Gu, T.; Cheng, L.; Li, X.; Han, G.; Liu, Z. Porous Pt nanoparticles loaded with doxorubicin to enable synergistic Chemo-/Electrodynamics Therapy. *Biomaterials* **2020**, *255*, 120202. [[CrossRef](#)]
139. Zhu, Y.; Li, W.; Zhao, X.; Zhou, Z.; Wang, Y.; Cheng, Y.; Huang, Q.; Zhang, Q. Hyaluronic Acid-Encapsulated Platinum Nanoparticles for Targeted Photothermal Therapy of Breast Cancer. *J. Biomed. Nanotechnol.* **2017**, *13*, 1457–1467. [[CrossRef](#)]
140. Zhang, X.F.; Liu, Z.G.; Shen, W.; Gurunathan, S. Silver Nanoparticles: Synthesis, Characterization, Properties, Applications, and Therapeutic Approaches. *Int. J. Mol. Sci.* **2016**, *17*, 1534. [[CrossRef](#)]
141. Kim, S.; Ryu, D.-Y. Silver nanoparticle-induced oxidative stress, genotoxicity and apoptosis in cultured cells and animal tissues. *J. Appl. Toxicol.* **2013**, *33*, 78–89. [[CrossRef](#)]
142. Holmila, R.J.; Vance, S.A.; King, S.B.; Tsang, A.W.; Singh, R.; Furdul, C.M. Silver Nanoparticles Induce Mitochondrial Protein Oxidation in Lung Cells Impacting Cell Cycle and Proliferation. *Antioxidants* **2019**, *8*, 552. [[CrossRef](#)]
143. Park, T.; Lee, S.; Amatya, R.; Cheong, H.; Moon, C.; Kwak, H.D.; Min, K.A.; Shin, M.C. ICG-Loaded PEGylated BSA-Silver Nanoparticles for Effective Photothermal Cancer Therapy. *Int. J. Nanomed.* **2020**, *15*, 5459–5471. [[CrossRef](#)]
144. Zhang, J.; Zhao, B.; Chen, S.; Wang, Y.; Xiao, H. Near-Infrared Light Irradiation Induced Mild Hyperthermia Enhances Glutathione Depletion and DNA Interstrand Cross-Link Formation for Efficient Chemotherapy. *ACS Nano* **2020**, *14*, 14831–14845. [[CrossRef](#)]
145. Awasthi, P.; An, X.; Xiang, J.; Kalva, N.; Shen, Y.; Li, C. Facile synthesis of noncytotoxic PEGylated dendrimer encapsulated silver sulfide quantum dots for NIR-II biological imaging. *Nanoscale* **2020**, *12*, 5678–5684. [[CrossRef](#)]
146. Chong, Y.; Huang, J.; Xu, X.; Yu, C.; Ning, X.; Fan, S.; Zhang, Z. Hyaluronic Acid-Modified Au–Ag Alloy Nanoparticles for Radiation/Nanozyme/Ag⁺ Multimodal Synergistically Enhanced Cancer Therapy. *Bioconjugate Chem.* **2020**, *31*, 1756–1765. [[CrossRef](#)]
147. Zhang, X.-S.; Xuan, Y.; Yang, X.-Q.; Cheng, K.; Zhang, R.-Y.; Li, C.; Tan, F.; Cao, Y.-C.; Song, X.-L. A multifunctional targeting probe with dual-mode imaging and photothermal therapy used in vivo. *J. Nanobiotechnology* **2018**, *16*, 42. [[CrossRef](#)]

148. Liu, M.; Peng, Y.; Nie, Y.; Liu, P.; Hu, S.; Ding, J.; Zhou, W. Co-delivery of doxorubicin and DNAzyme using ZnO@polydopamine core-shell nanocomposites for chemo/gene/photothermal therapy. *Acta Biomater.* **2020**, *110*, 242–253. [[CrossRef](#)]
149. Sun, Y.; Yan, C.; Xie, J.; Yan, D.; Hu, K.; Huang, S.; Liu, J.; Zhang, Y.; Gu, N.; Xiong, F. High-Performance Worm-like Mn-Zn Ferrite Theranostic Nanoagents and the Application on Tumor Theranostics. *ACS Appl. Mater. Interfaces* **2019**, *11*, 29536–29548. [[CrossRef](#)] [[PubMed](#)]
150. Thakur, N.S.; Patel, G.; Kushwah, V.; Jain, S.; Banerjee, U.C.; Thakur, N.S. Facile development of biodegradable polymer-based nanotheranostics: Hydrophobic photosensitizers delivery, fluorescence imaging and photodynamic therapy. *J. Photochem. Photobiol. B* **2019**, *193*, 39–50. [[CrossRef](#)] [[PubMed](#)]
151. Anselmo, A.C.; Mitragotri, S. Nanoparticles in the clinic: An update post COVID-19 vaccines. *Bioeng. Transl. Med.* **2021**, *6*, e10246. [[CrossRef](#)] [[PubMed](#)]
152. Rodallec, A.; Benzekry, S.; Lacarelle, B.; Ciccolini, J.; Fanciullino, R. Pharmacokinetics variability: Why nanoparticles are not just magic-bullets in oncology. *Crit. Rev. Oncol. Hematol.* **2018**, *129*, 1–12. [[CrossRef](#)] [[PubMed](#)]
153. Wilhelm, S.; Tavares, A.J.; Dai, Q.; Ohta, S.; Audet, J.; Dvorak, H.F.; Chan, W.C.W. Analysis of nanoparticle delivery to tumours. *Nat. Rev. Mater.* **2016**, *1*, 16014. [[CrossRef](#)]
154. Shi, J.; Kantoff, P.W.; Wooster, R.; Farokhzad, O.C. Cancer nanomedicine: Progress, challenges and opportunities. *Nat. Rev. Cancer* **2017**, *17*, 20–37. [[CrossRef](#)]
155. Rastinehad, A.R.; Anastos, H.; Wajswol, E.; Winoker, J.S.; Sfakianos, J.P.; Doppalapudi, S.K.; Carrick, M.R.; Knauer, C.J.; Taouli, B.; Lewis, S.C. Gold nanoshell-localized photothermal ablation of prostate tumors in a clinical pilot device study. *Proc. Natl. Acad. Sci. USA* **2019**, *116*, 18590–18596. [[CrossRef](#)]
156. Bayda, S.; Hadla, M.; Palazzolo, S.; Riello, P.; Corona, G.; Toffoli, G.; Rizzolio, F. Inorganic Nanoparticles for Cancer Therapy: A Transition from Lab to Clinic. *Curr. Med. Chem.* **2018**, *25*, 4269–4303. [[CrossRef](#)]
157. Kumthekar, P.; Ko, C.H.; Paunesku, T.; Dixit, K.; Sonabend, A.M.; Bloch, O.; Tate, M.; Schwartz, M.; Zuckerman, L.; Lezon, R. A first-in-human phase 0 clinical study of RNA interference-based spherical nucleic acids in patients with recurrent glioblastoma. *Sci. Transl. Med.* **2021**, *13*, eabb3945. [[CrossRef](#)]
158. Kumthekar, P.; Rademaker, A.; Ko, C.; Dixit, K.; Schwartz, M.A.; Sonabend, A.M.; Sharp, L.; Lukas, R.V.; Stupp, R.; Horbinski, C.; et al. A phase 0 first-in-human study using NU-0129: A gold base spherical nucleic acid (SNA) nanoconjugate targeting BCL2L12 in recurrent glioblastoma patients. *J. Clin. Oncol.* **2019**, *37* (Suppl. S15), 3012. [[CrossRef](#)]